AFIT/GE/ENG/99M-21

LOW GRAZING ANGLE TERRAIN BACKSCATTERING COEFFICIENT (σ^0) GENERATOR

THESIS

William N. O'Connor
Captain, USAF
AFIT/GE/ENG/99M-21

Approved for public release; distribution unlimited

REPORT DOCUMENTATION PAGE

Form Approved
OMB No. 0704-0188

1. AGENCY USE ONLY *(Leave blank)*	2. REPORT DATE	3. REPORT TYPE AND DATES COVERED
	March 1999	Master's Thesis

4. TITLE AND SUBTITLE
LOW GRAZING ANGLE TERRAIN BACKSCATTERING COEFFICIENT GENERATOR

5. FUNDING NUMBERS

6. AUTHOR(S)
William N. O'Connor, Captain, USAF

7. PERFORMING ORGANIZATION NAME(S) AND ADDRESS(ES)
Air Force Institute of Technology,
2950 P Street
WPAFB, OH 45433-7765

8. PERFORMING ORGANIZATION REPORT NUMBER
AFIT/GE/ENG/99M-21

9. SPONSORING/MONITORING AGENCY NAME(S) AND ADDRESS(ES)
AFRL/SNAS
Attn: Capt Kelce Wilson
2010 Fifth Street, Bldg 23, Area B
Wright-Patterson AFB, OH 45433
(937) 255-6329/DSN 785-6329

10. SPONSORING/MONITORING AGENCY REPORT NUMBER

11. SUPPLEMENTARY NOTES
Dr. Vittal Pyati / 255-3636 x4576, DSN 785-3636 x4576 / vittal.pyati@afit.af.mil

12a. DISTRIBUTION AVAILABILITY STATEMENT
Approved for public release; distribution unlimited

12b. DISTRIBUTION CODE

13. ABSTRACT *(Maximum 200 words)*

A near-horizon probabilistic terrain backscatter coefficient generator is introduced, combining modified sea-state curves with Weibull-type probability density functions. A total of nine terrain type classifications (soils & rocks, trees, grasses, shrubs, short vegetation, roads, urban areas, dry snow, and wet snow) are supported, for seven radar bands (L, S, C, X, Ku, Ka, and W), and both linear (HH, VV) and cross (HV, VH) polarizations. The Weibull functions are based on measured sigma and match the published data. The functions also provide a probabilistic nature to the generator. Modified sea state curves are used in place of the Weibull functions for near-horizon incidence angles due to the dearth of measured data at this range. The sea state approach is based on the theory that for sigma, similar surface roughness of two different terrain types results in similar sigma curve shapes. Generator testing and validation used available measured sigma for three terrain types. The testing did not reject the modified sea curve usage and allowed system implementation for the remaining terrain types.

14. SUBJECT TERMS
Radar, Radar Backscatter, Low Grazing Angle, Ground Clutter, Clutter Suppression

15. NUMBER OF PAGES
86

16. PRICE CODE

17. SECURITY CLASSIFICATION OF REPORT	18. SECURITY CLASSIFICATION OF THIS PAGE	19. SECURITY CLASSIFICATION OF ABSTRACT	20. LIMITATION OF ABSTRACT
Unclassified	Unclassified	Unclassified	UL

The views expressed in this thesis are those of the author and do not reflect the official policy or position of the Department of Defense or the U.S. Government.

AFIT/GE/ENG/99M-21

LOW GRAZING ANGLE TERRAIN BACKSCATTERING COEFFICIENT (σ°) GENERATOR

William N. O'Connor, B.S.

Captain, USAF

Approved:

Vittal P. Pyati — 3 Mar 99

Dr. Vittal P. Pyati
Thesis Advisor — Date

4 Mar 99

Maj. Michael A. Temple, Ph.D.
Committee Member — Date

3/3/99

Dr. Andrew J. Terzuoli
Committee Member — Date

AFIT/GE/ENG/99M-21

LOW GRAZING ANGLE TERRAIN BACKSCATTERING COEFFICIENT (σ^0) GENERATOR

THESIS

Presented to the Faculty of the Graduate School of Engineering

of the Air Force Institute of Technology

Air University

Air Education and Training Command

In Partial Fulfillment of the Requirements for the

Degree of Master of Science in Electrical Engineering

William N. O'Connor, B.S.

Captain, USAF

March 1999

Acknowledgments

I would like to thank my thesis advisor, Dr. Vittal Pyati, and my thesis committee, Maj Michael Temple and Dr. Andrew Terzuoli, for their guidance and assistance during this project. They have shown great patience and foresight, and many times they have kept me from going down a wrong path.

My sponsor, Capt Kelce Wilson, was no less important to the success of this research. His knowledge and expertise on this subject helped greatly and I appreciate all the time he took from his busy schedule to answer questions or to listen to crazy ideas.

The guys of the Communications Lab, Rick, Andy, Andy, Perry, Todd, John, Dan, Patrick, Dave, and Mike. Together, we spent many a sleepless night working on papers and homework while always keeping alive a sense of humor. Even with all the hard work and pain we went through, I will miss these times.

Finally, to my family, Neil, Patricia, Patrick, Michael, and the pets; Thank you for being the support I could always depend on. Words can not fully describe what you have done for me, so I will simply say, Thank you.

Table of Contents

List of Figures

List of Tables

Preface

This research develops a near-horizon/low-grazing angle backscattering coefficient (σ^o) generator for several radar bands, types of terrain, and wave polarizations.

The low-grazing σ^o generator is a fusion of two separate models: a low-incidence angle σ^o generator that returns the probabilistic means of σ^o for a given terrain, frequency, and incidence angle; and a low-grazing sea surface backscatter model. The theory that low-grazing angle σ^o depends more on surface roughness than on surface composition allows for this sea model usage.

The generating function is implemented in MATLAB®, and is updateable when new low-grazing data becomes available. The function is available in FORTRAN from the author.

Abstract

A near-horizon probabilistic terrain backscatter coefficient (σ^o) generator is introduced, combining modified sea-state curves with Weibull-type probability density functions. A total of nine terrain type classifications (soils & rocks, trees, grasses, shrubs, short vegetation, roads, urban areas, dry snow, and wet snow) are supported, for seven radar bands (L, S, C, X, Ku, Ka, and W), and both linear (HH, VV) and cross (HV, VH) polarizations. The Weibull functions are based on measured σ^o and match the published data. The functions also provide a probabilistic nature to the generator. Modified sea state curves are used in place of the Weibull functions for near-horizon incidence angles ($75^o - 90^o$) due to the dearth of measured data at this range. The sea state approach is based on the theory that for σ^o, similar surface roughness of two different terrain types results in similar σ^o curve shapes. Generator testing and validation used available measured σ^o at 85^o for three terrain types. The testing did not reject the modified sea curve usage and allowed system implementation for the remaining terrain types.

LOW GRAZING ANGLE TERRAIN

BACKSCATTERING COEFFICIENT (σ^o) GENERATOR

I. Introduction

1.1 Background

The backscattering coefficient, σ^o, is a measure of the electromagnetic energy scattered by a distributed target in the receiver direction. In general, σ^o depends upon the target's shape, dielectric constant, viewing geometry, and the attributes of the incident and scattered electromagnetic waves (wavelength, polarization, and incidence angle) [1].

For terrain, the value of σ^o depends upon its features, such as water content, composition, degree of roughness, and the location of scattering centers. Generally, terrain scattering centers are randomly distributed and vary in position with frequency and incidence angle, giving σ^o its random quality [1]. The variation of the backscattering coefficient justifies its description as a mean value calculated from several measurements at a specific incidence angle, frequency, and wave polarization. The associated standard deviation of the measurements may be calculated and used as well.

For low-grazing angles near the horizon, the data available is very scant. Because of this lack of data, deterministic models have been developed based on small subsets of the available data that would fit the determined model.

The terms "low-grazing angle" and "high-incidence angle" are used interchangeably. This exchange in terms is owed to the popularity of the "low-grazing" term in the scientific community and in early σ^o research while the term "high-incidence" is used by

the two primary sources of data. In this work, for continuity with past studies, "low-grazing" will describe the region of research and the measured data. However, all angles described use incidence nomenclature for continuity with the two data sources (University of Michigan, RADLAB and Army Research Laboratory, ARL)

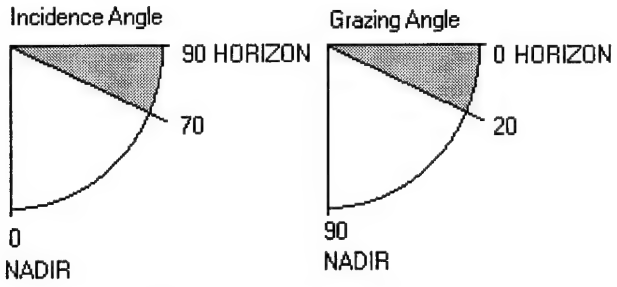

Figure 1. Grazing angle vs. Incidence Angle

1.2 Problem Statement

Develop a low-grazing/near-horizon σ^o generator for several terrain types, frequency bands, and wave polarizations. This generator will operate in conjunction with the backscatter coefficient generator [2] developed for incidence angles $0^o \leq \theta \leq 80^o$. The generator will output data for the nine terrain types specified by RADLAB [1], seven radar bands, and three wave polarizations. When new low-grazing angle data becomes available, the generator must be updateable and generate σ^o's with the same probabilistic distributions as the measured data.

1.3 Summary of Current Knowledge

Very little measured data is available for low-grazing angle σ^o measurements. Vast majority of studies have created deterministic models based only on the limited amount of data they measured [3, 4, 5]. Army Research Laboratory (ARL) measured W-band

backscatter coefficients from $85^\circ \leq \theta \leq 89^\circ$ for European-type terrain (trees, grass fields, dirt, and snow) [6]. Unfortunately, the measurement sample sizes and number of terrain types measured were limited. RADLAB has been compiling σ^o's from numerous studies and creating a large σ^o database complete with means and standard deviations for numerous terrain types and incidence angles. The RADLAB data compilation is the basis for the lower incidence-angle σ^o generator being concurrently developed [2]. However, there is no data available from RADLAB for incidence angles $\theta > 80^\circ$.

1.3.1 Beckmann Method.

In general, when low-grazing data was limited or unavailable, almost all prior models use a squared sinusoid to fill in the data near the horizon.

$$\sigma^o(\theta) = \sigma^0(0) \cdot \sin^2\theta \quad \text{(for grazing angles)} \qquad (1)$$

$$\sigma^o(\theta) = \sigma^0(0) \cdot \cos^2\theta \quad \text{(for incidence angles)} \qquad (2)$$

where $\sigma^o(0)$ is the terrain σ^o value at nadir.

While this method has a good fit of measured data for a limited number of terrain types and incidence angles, it has been rejected for its behavior at the horizon [3, 4, 6]. When θ is at the horizon ($\theta = 0^\circ$ for grazing, 90° for incidence), σ^o equals zero. A number of studies that have measured σ^o at the horizon have detected a small amount of return energy [3, 4, 7]. This return energy usually is due to a distant object, or objects, in view of the receiver (a tree, long grass, sea waves, or a distant building). Figure 2 demonstrates this condition.

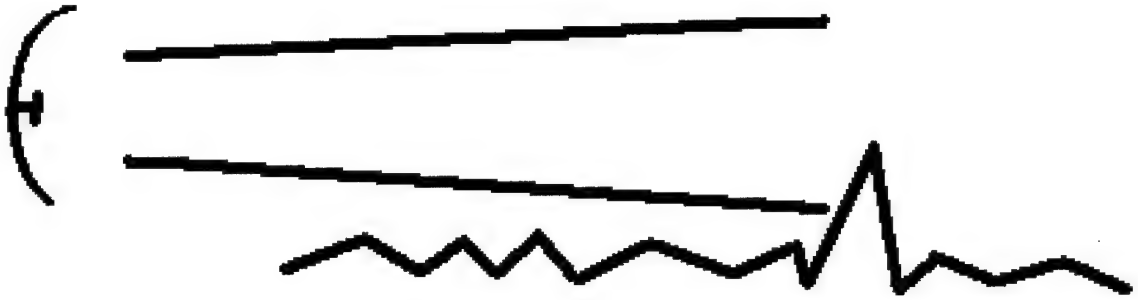

Figure 2. Radar at Horizon receiving a distant object

1.4 Thesis Overview

A backscatter generator for incidence angles $0^\circ < \theta < 80^\circ$, based on the probabilistic distribution of measured σ^o's , is available [2] (to be referred as the Wilson/Mediavilla Generator or σ_{WM} **GEN**). By theorizing that at low-grazing angles, σ^o is more affected by surface roughness, a widely accepted sea backscatter model is used to generate backscatter curves for incidence angles up to, and including, horizon. The overall value or "height" of the curve is set by σ_{WM} **GEN** and the sea model will extrapolate the rest of the desired σ^o's. [2]

Terrain roughness is specified by sea wave height. The roughness-wave height correlation is done using available measured data as a validating target. In situations where data is unavailable, the wave height will be set by either the wave height given for the specified terrain at a higher frequency (usually W-band since the only available data is in W-band) or by using a Rayleigh roughness model. [5]

Chapter 2 reviews the theory behind the measurement of σ^o and a method to theoretically measure the effect on low-grazing angle σ^o of surface roughness vs surface

composition. The chapter concludes with an analysis of the ARL data and shows how it relates to the RADLAB data used in σ_{WM} **GEN**.

Chapter 3 will introduce the sea backscatter model and validation of the model using σ_{WM} **GEN** and the ARL data.

Selected σ^o generations for the near-horizon incidence angle range ($60^o \leq \theta \leq 90^o$) will be graphed in chapter 4.

Conclusions and recommendations for future study will sum up chapter 5 and this research.

II. Theory

2.1 Overview

Since the beginnings of radar, the detection of unwanted objects, or "clutter", has interfered with the measurement of desired targets. The problem is that there is no one type of clutter. An airport search radar tracking aircraft would call weather returns clutter, while a weather radar would want to remove the clutter caused by aircraft. Furthermore, a space surveillance system would consider aircraft and weather returns to be unwanted clutter. Thus, this gives rise to the saying: *One radar's clutter is another radar's target* [8].

In this research, our target is ground clutter, or now known as terrain backscatter (σ^o). Backscatter is transmitted energy reflected by ground, or surface, elements back to the radar receiver [9]. The amount of energy received varies with the terrain type and the angle the transmitted beam hits the surface. On most radar systems, backscatter is just an annoyance to be worked around. However, in some applications, mostly military, backscatter can mask targets, making the targets more difficult to detect [10].

To counteract the backscatter effects on ground-based radar systems, one of two methods is usually applied. The first method uses zero-Doppler effects to identify and remove clutter effects [9]. This means that the system removes any return that does not appear to be moving. While this method is effective in removing clutter, it has been found that slow moving targets, in ground applications, are also removed, degrading the effectiveness of the system [10].

A new method that has started to take hold is predicting the backscatter for a given terrain surface at a given angle. Because this method requires previous knowledge of

backscatter energy from specific terrain types as well as knowledge of the terrain surface that will be in the radar bore-site, this method has been slow in gaining acceptance. However, with the availability of DTED (Digital Terrain Elevation Data) maps for the world as well as the development of backscatter models, this method is becoming more and more prevalent [5, 10, 11].

This method is not without its problems. Because of the number of variables that can affect backscatter (terrain type, surface roughness, frequency, and moisture content to name a few), the actual energy return can vary from measurement to measurement [10, 11]. Usually, the amount of energy recorded is a mean of the measurements. Unfortunately, the models that are developed from the recorded data are usually deterministic (ie. for a given angle, terrain type, frequency, etc... the same result is returned). The lack of a probabilistic nature in the model does not reflect the actual measured return energy [2, 10].

As more and more data is collected and recorded, probabilistic models have started to develop. These models add the variance that exists in backscatter energy. Most notably, the data collection from RADLAB of the University of Michigan has resulted in not fewer than 3 probabilistic models (RADLAB, Wilson, & Wilson/Mediavilla) [1, 2, 10]. Unfortunately, this data collection only exists in the incidence angle range from $0^\circ < \theta < 80^\circ$. The Army Research Laboratory (ARL) measured backscatter energy in the "shadow" or grazing region ($80^\circ \leq \theta \leq 90^\circ$) for a small number of terrain types at 95 GHz [6].

This research will develop a probabilistic model for the grazing region by combining an available grazing angle deterministic model with one of the above mentioned probabilistic models (Wilson/Mediavilla) [2].

In this chapter, a sample σ^o will be calculated from the radar range equation and the effect of terrain on σ^o will be documented. Then, three sample surfaces, two random sets of grass or trees, and one sea waves set, of varying heights will demonstrate geometric and reflectivity effects on σ^o in the grazing region. Then, analysis on the only available "shadow" region data will be discussed. Finally, a review of previous terrain models and why they were rejected in favor of a sea model will be done.

2.2 Calculation of Backscatter Coefficient (σ^o)

Because many factors affect the magnitude of the backscatter, it is best to start with the basic radar range equation and work to the backscatter measurement. While deriving the equations, it will become clear why a probabilistic generation of σ^o would be better than a deterministic model calculation.

Starting with an antenna radiating in free space at a wavelength, λ, and signal power, P_t transmitting isotropocially, the power density, P, or the power per unit area, at a range R from the antenna is calculated to be:

$$P = \frac{P_t}{4\pi R^2} \tag{3}$$

Since radars use directive antennas to increase range, antenna gain, G_t, is multiplied by P to get the power density for a directed antenna, P_g. Gain from the antenna is defined as:

$$G_t = 4\pi\left(A_e / \lambda^2\right) \tag{4}$$

$$P_g = P \cdot G_t \tag{5}$$

with A_e being the aperture or receiver part of an antenna. The power incident at a point at distance R from the transmitting antenna, and on its boresight, is [4]:

$$P_r = P_g \cdot A_e \tag{6}$$

$$P_r = \frac{P_t G^2 \lambda^2}{(4\pi)^2 R^2} \tag{7}$$

The radar cross section, (RCS) also known as σ, of a target may be defined as "the area intercepting that amount of power which, when scattered isotropically, produces an echo equal to that received from the object" [12]. Simplified, it implies a measure of power that would be returned by a perfect reflector at that range. The power received from a target with a RCS of σ, P_σ, can be calculated by multiplying the antenna power density by the power density of a target radiating isotropically:

$$P_\sigma = \frac{P_t G}{4\pi R^2} \cdot \frac{\sigma}{4\pi R^2} \tag{8}$$

assuming a monostatic radar where the transmit and receive antennas are co-located. The power density at the receive antenna is simply calculated as:

$$P_r = P_\sigma A_e \tag{9}$$

This results in the basic radar range equation below:

$$P_r = \frac{P_t G^2 \lambda^2}{(4\pi)^3 R^4} \sigma \tag{10}$$

where P_r = Received Power, P_t = Transmitted Power, G = Antenna Gain, λ = wavelength, R = range from antenna to target, and σ = the target's radar cross section (RCS) at that wavelength [4]. Because the available measured data is overwhelmingly monostatic, the bistatic case is ignored.

The RCS, σ, is usually normalized for an ideal target or surface and has other dependencies other than wavelength [4]. This will discussed in section 2.3.

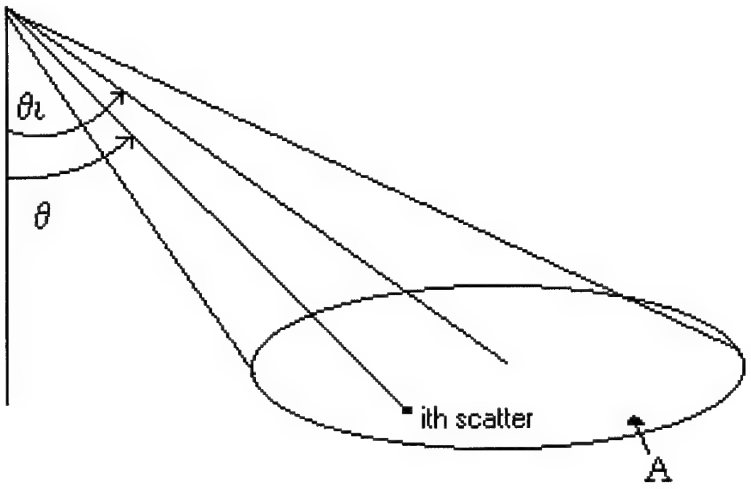

Figure 3. Illumination of an area

Using the radar range equation and integrating over an area A containing N scatterers:

$$P_N(\theta) = \iint_A \frac{P_t G^2 \lambda^2}{(4\pi)^3 R^4} \cdot \sigma_i dA \tag{11}$$

σ_i i = 1, 2, 3, …, N scatterers

and narrowing down the beamwidth such that it approaches 0, σ becomes σ^o and the integral collapses to a single system constant K [1].

$$P_N(\theta) = K\sigma^0 \tag{12}$$

This constant can be calculated for each testing radar system to allow for continuity between separate tests and radar systems. If the calculation is not performed, and K not compensated, an error referred to as Registration error is introduced. The only way to

remove this error is to have a complete listing of all of the measuring radar's system parameters.

Both RADLAB and ARL attempted K calculations to remove errors [13]. It is assumed that all registration errors between the RADLAB data and ARL data equal zero. For future data measurements, however, at least a factor of K should be included with the published data for confirmation of registration error removal.

2.3 Terrain Dependence of σ^o

Since the constant K of Equation (12) can be calculated and fixed, the return power depends on σ^o. The amount of variance of σ^o for most terrain types makes it very difficult to create a single deterministic equation and ultimately is the reason behind the probabilistic modeling approach that is used.

The value of σ^o is dependent on surface moisture content as demonstrated by RADLAB [7]. The higher the moisture that is in the surface, the higher the measured σ^o. With a change in soil moisture from desert conditions to very moist ground, RADLAB measured a σ^o change of 5-7 dB [7].

In the shadow region, however, the σ^o dependence on the incidence angle becomes the dominating factor. The change in σ^o varies between 5-20 dB from 70^o to 90^o. Below 70^o, however, σ^o flattens out to a small change in dB until $\theta \cong 30^o$ [1, 3].

The interaction between σ^o (or the shape of the overall σ^o curve) appears to be dependent on the surface roughness. If the surface is mostly smooth (snow, asphalt, dirt), the curve plateaus and then quickly drops as the incidence angle is increased past 70^o. If

the surface is rough (trees, grass, rocks), then the curve will gradually drop as the incidence angle is increased. In one terrain case, urban areas, the curve remains constant, or drops a little, no matter what the incidence angle is. This is expected due to the number of corner and angle reflectors that can be found in buildings and structures [2].

2.4 Simulated Surface Model

As stated above, a terrain's roughness appears to have a large affect on the shape or percentage change in σ^o at low-grazing angles. Meanwhile, the terrain composition appears to affect only the overall value of σ^o at a given incidence angle (or "height"), not its relationship to its neighboring values (or "shape of the curve"). By properly modeling these effects, an innovative method is developed for modeling σ^o at all incidence angles.

If the curve has the same percentage drop in values for terrain of the same roughness, but not of the same surface composition or material makeup, then a model for one surface type could be substituted for another surface type. This theory can tested by creating random surfaces of varying heights and assigning electrical constants (permittivity and conductivity) to the surface facets [14].

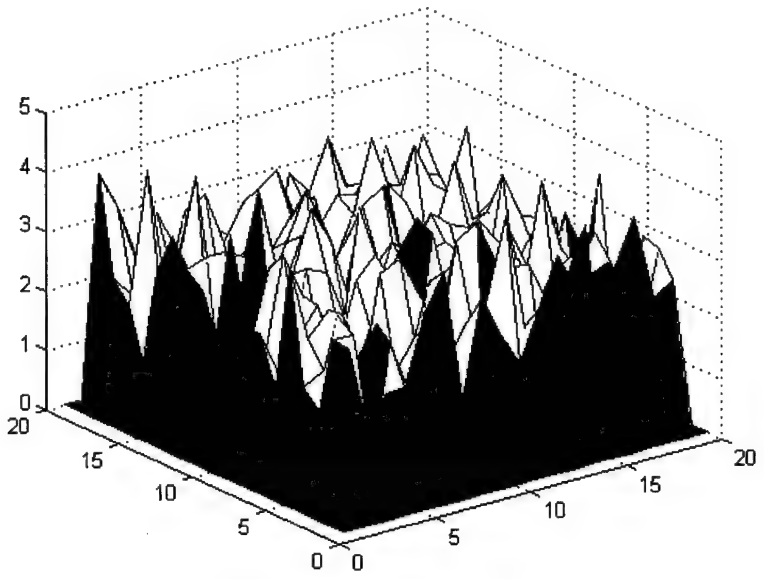

Figure 4. Random Surface

2.4.1 Rough Surface.

For rough terrain, as the incidence angle changes, the change in σ^o is primarily dependent on two effects, geometric changes and reflectivity changes [13]. Geometric changes can be measured in the number of facets that are visible for a given incidence angle and the average slope of the facets. Reflectivity changes can be modeled by Fresnel reflection coefficients calculated for each facet as given by Beckmann [14].

Each visible facet can be compared to a scattering point. As the number of visible facets increases with each change in incidence angle, the number of scatterers increase, increasing overall σ^o.

The average slope of the facets can be compared to the amount of energy reflected back to the receiver. As facet face approaches to normal incidence with the receiver, the amount of energy reflected back to the receiver increases. Likewise, as the facet approaches grazing, the energy reflected back decreases, reducing σ^o. The Fresnel

reflection coefficients calculate the amount of energy each facet receives and with the average slope, can calculate the amount of energy reflected back to the receiver [14].

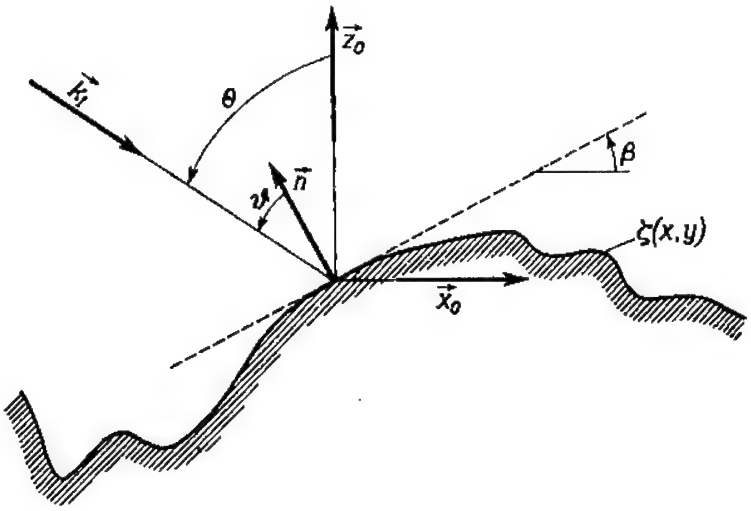

Figure 5. Scattering off of Random Surface [14]

2.4.2 Fresnel Reflectivity Coefficients.

The coefficients depend on intersect angle, the electrical properties of the surface, and the polarization of the intersecting wave [14].

$$R^{+} = \frac{Y^2 \cos\vartheta - \sqrt{Y^2 - \sin^2\vartheta}}{Y^2 \cos\vartheta + \sqrt{Y^2 - \sin^2\vartheta}} \text{ Vertical Polarization} \qquad (13)$$

$$R^{-} = \frac{\cos\vartheta - \sqrt{Y^2 - \sin^2\vartheta}}{\cos\vartheta + \sqrt{Y^2 - \sin^2\vartheta}} \text{ Horizontal Polarization} \qquad (14)$$

$$Y = \sqrt{\frac{\varepsilon_{re}}{\mu_{re}}} \text{ Normalize admittance} \qquad (15)$$

The geometric and reflectivity effects on σ^o can be modeled in the following way: First, create a random rough surface with a given average height. Then, for incidence

angles from $60^{o} < \theta < 90^{o}$, calculate the number of facets that are visible, the average slope of each facet, and the vertical and horizontal Fresnel reflectivity coefficients for each facet. Finally, calculate a total "σ^{o}" from the coefficients, number of facets, and average slope.

2.4.3 Random Surface.

For this set of graphs, the normalized admittance, Y, is calculated for grass, Y = 2.24 [4].

The results are as follows:

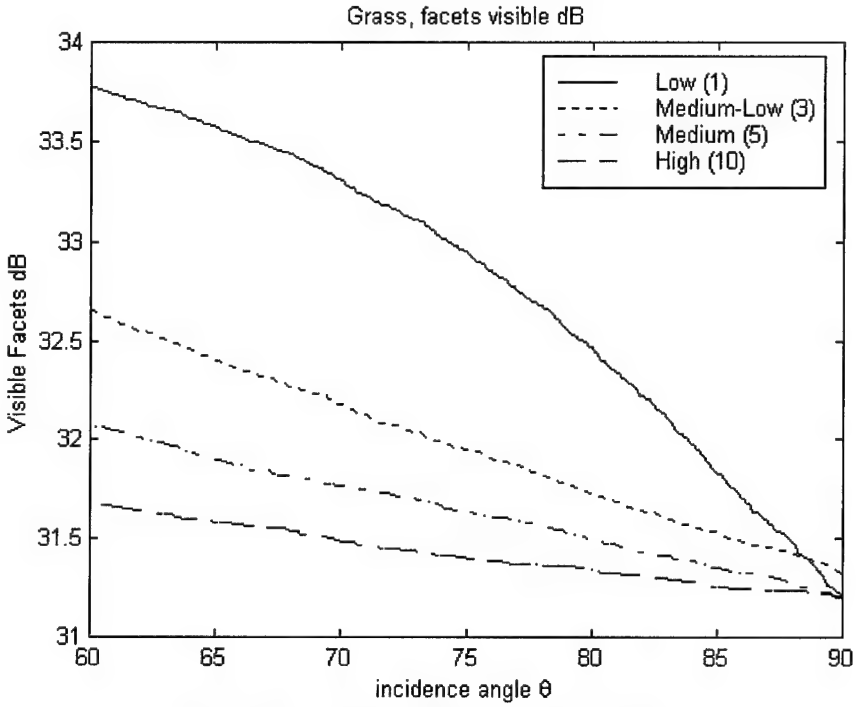

Figure 6. Visible Facets in dB (Grass)

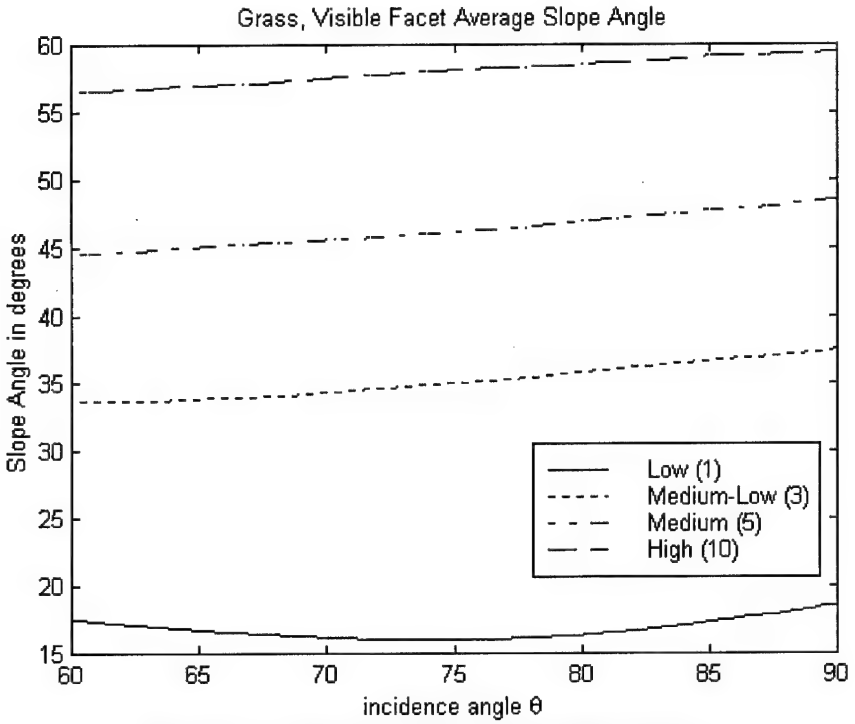

Figure 7. Average Visible Facet Slope Angle (Grass)

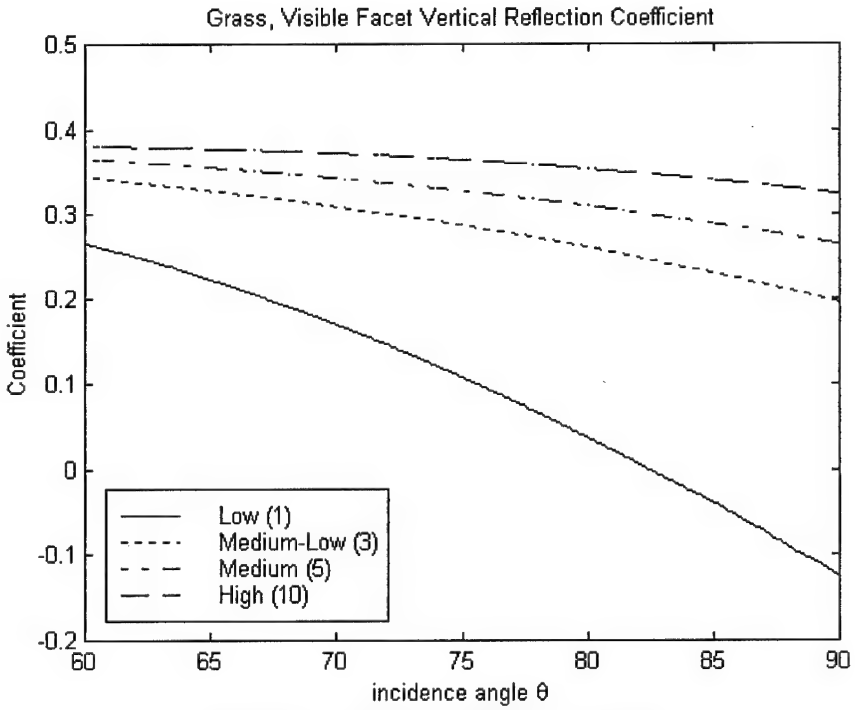

Figure 8. Vertical Coefficient (Grass)

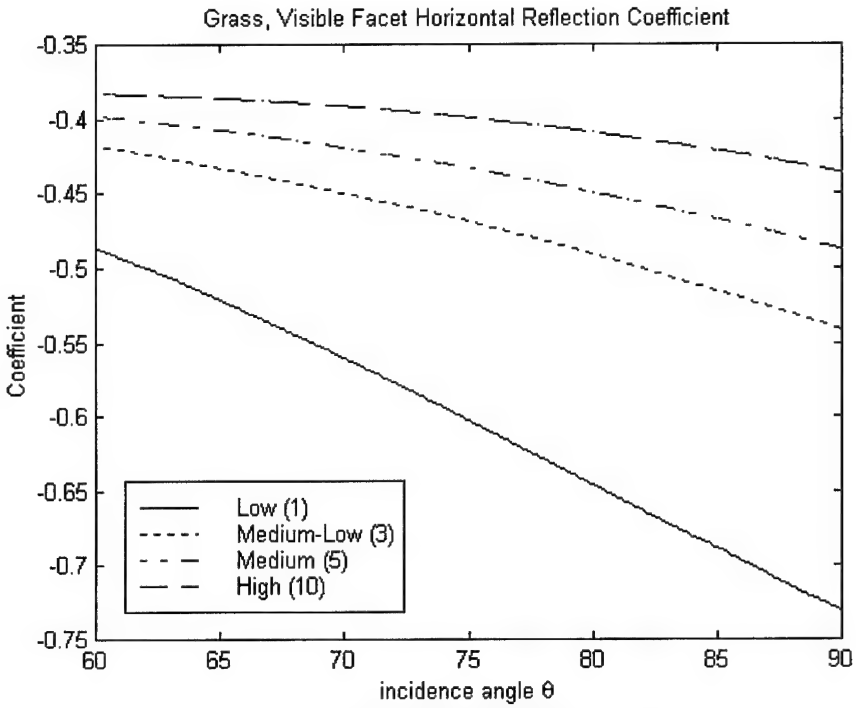

Figure 9. Horizontal Coefficient (Grass)

The overall values of each graph are not of concern in this study. The interaction of the values for each surface determines the value of "σ^o". By calculating the percentage change of each factor (visible facets, average slope angle, & Fresnel coefficients), a pattern emerges that shows which factor changes the most and thus has the greatest effect on "σ^o" in the shadow region.

A graph of a theorized "σ^o", calculated for each angle as:

σ^o = (# of visible facets)*(Average facet slope)*(Vertical Coeff. + Horizontal Coeff.) (16)

allows for this analysis.

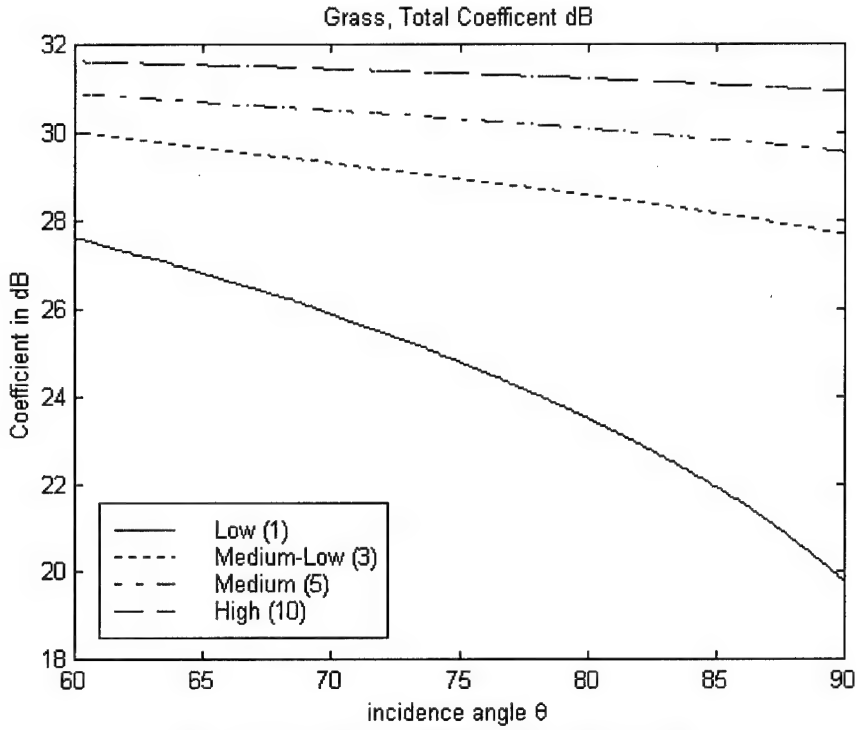

Figure 10. Total Coefficient in dB (Grass)

It is interesting to note that the curve shapes match very closely to the "σ^0" curve shapes in nature. For a relatively smooth surface (Low), the curve drops quickly. This curve shape has been seen in measurements of roads and flat ground. The rougher the surface, the flatter and less steep the curve becomes, as seen in the three other surfaces. This curve has been noticed in measurements of rougher surfaces, rocky ground, rough seas, and trees.

The effect of each factor is measured and compared to the other factors by taking a percent difference. Each percentage is calculated by taking the difference between the lowest and highest simulated measurements and dividing by a fixed value. The fixed value is the largest value each simulated measurement could obtain. For facets, at most 10,000 possible facets could be seen. For average slope, the value is 90^o. For the Fresnel

Coefficients, the value when the surface is normal to the radar beam is max. σ^o total is the exception with a simple percentage change of (max-min)/max. The results follow in Table 1.

	Low	Low-Medium	Medium	High
Δ% Visible Facets	79.9 %	35.7 %	22.1 %	11.7 %
Δ% Ave. Slope	2.8 %	4.3 %	4.5 %	3.4 %
Δ% Vert. Coeff. max mag. (0.39)	38.0 %	15.0 %	9.1 %	5.0 %
Δ% Hori. Coeff. max mag. (-0.39)	19.4 %	11.3 %	7.8 %	4.7 %
Δ% σ^o Total	83.5 %	41.2 %	26.1 %	14.9 %

Table 1. Δ% Change in factors (Grass)

For each of the surface heights, the percent change in visible facets is the greatest and appears to be the primary effect on the percent change in total σ^o. If this pattern continues for other values of Y as well as for different type of surface shapes (sea surfaces), it would imply that the theory that σ^o is mostly affected by surface roughness at low-grazing angles would be correct.

2.4.4 Random Shrubs & Trees.

The next set of graphs is for Y calculated for shrubs (small average random height) and trees (large average random height), Y = 3.16. Again, the results are similar as before.

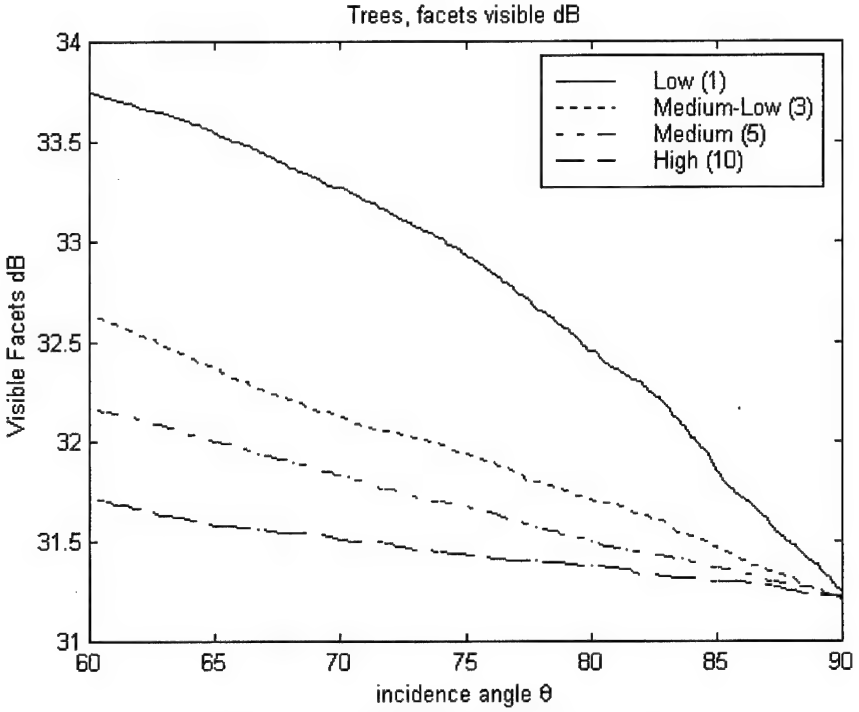

Figure 11. Visible Facets in dB (Trees)

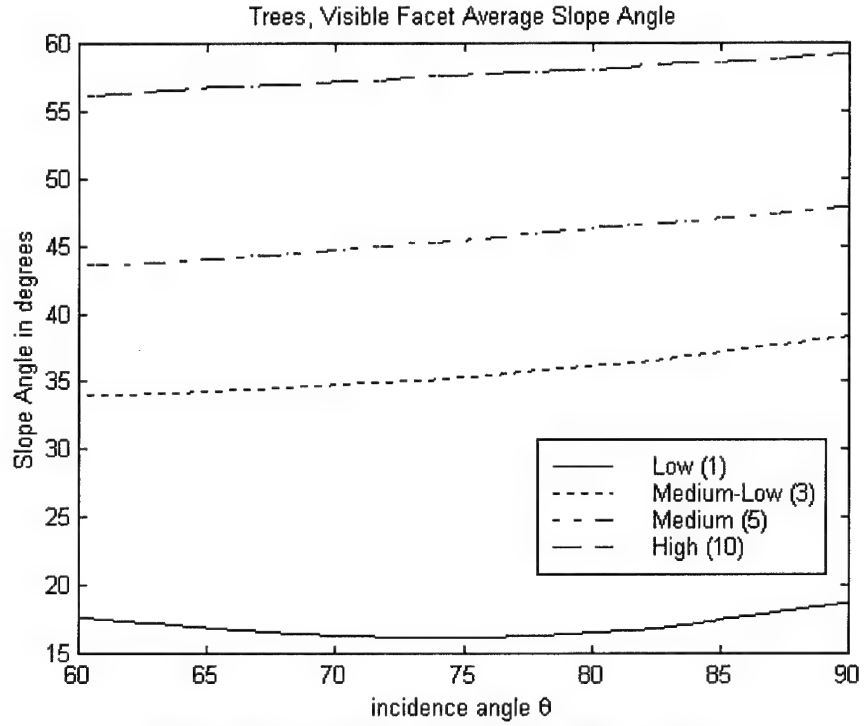

Figure 12. Average Visible Facet Slope Angle (Trees)

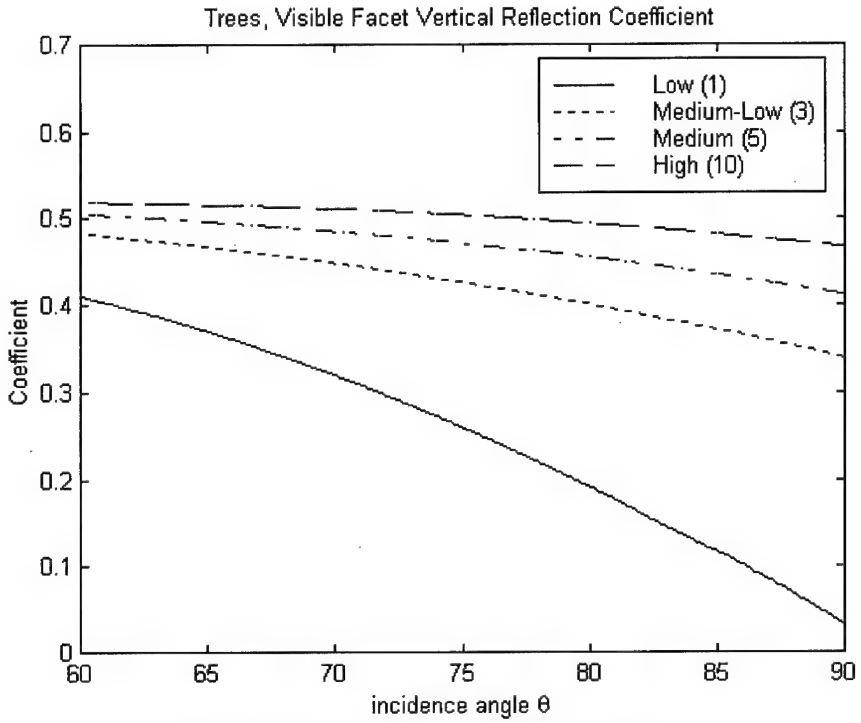

Figure 13. Vertical Coefficient (Trees)

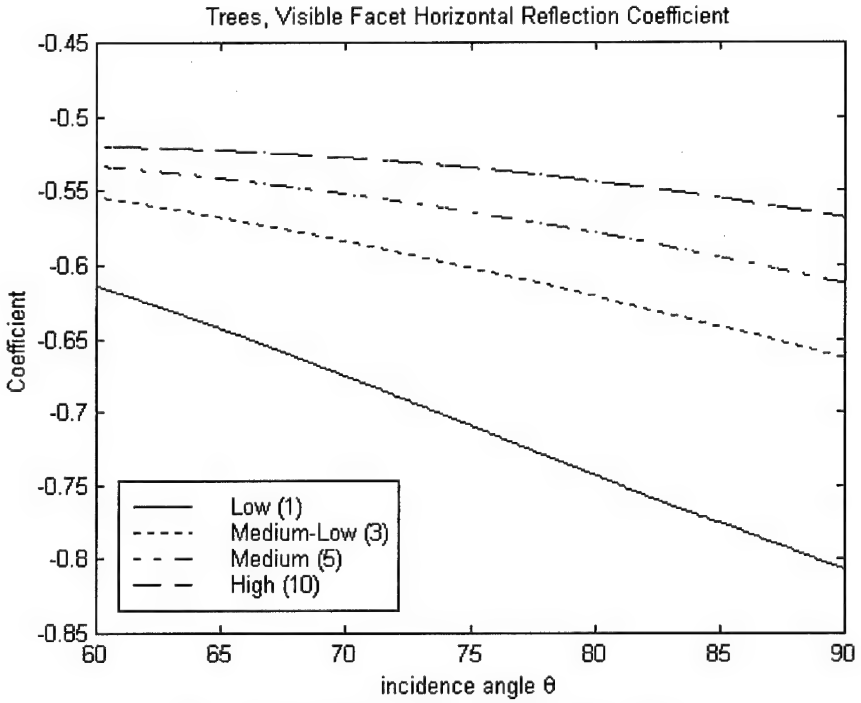

Figure 14. Horizontal Coefficient (Trees)

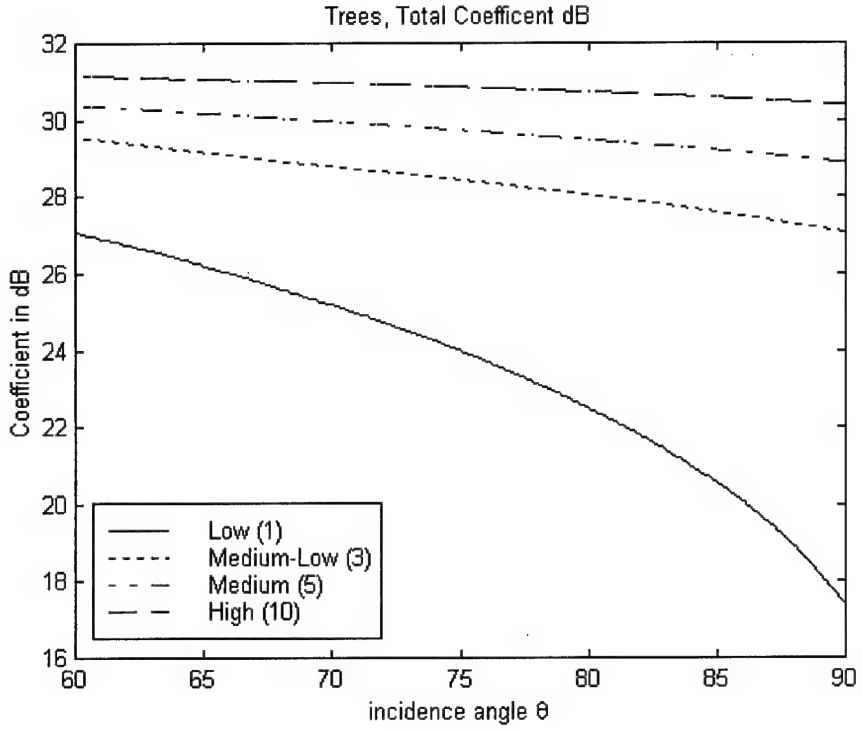

Figure 15. Total Coefficient in dB (Trees)

The results in Table 2 are calculated the same way as Table 1.

	Low	Low-Medium	Medium	High
Δ% Visible Facets	77.5 %	38.9 %	25.1 %	12.1 %
Δ% Ave. Slope	2.8 %	4.8 %	4.9 %	3.5 %
Δ% Vert. Coeff. max mag. (0.52)	37.7 %	14.4 %	9.3 %	5.1 %
Δ% Hori. Coeff. max mag (-0.52)	19.3 %	10.9 %	7.9 %	4.8 %
Δ% Total	89.1 %	43.5 %	29.4 %	16.3 %

Table 2. Δ% Change in factors (Trees)

As before, in the simulated grass surface, the simulated tree surface shows same larger percentage change in the number of visible facets compared to the change in average

slope and the coefficients. This supports the theory that "σ^{o}" is more affected by surface roughness.

2.4.5 Simulated Sea Surface.

The next test of this theory is to see if a non-random, periodic surface, such as sea waves, would exhibit the same behavior. If a simulated sea surface would exhibit similar changes in effects, that would allow use of a sea clutter generator to model the overall shape of the σ^{o} curve for terrain (ie. the change in σ from one angle to the next).

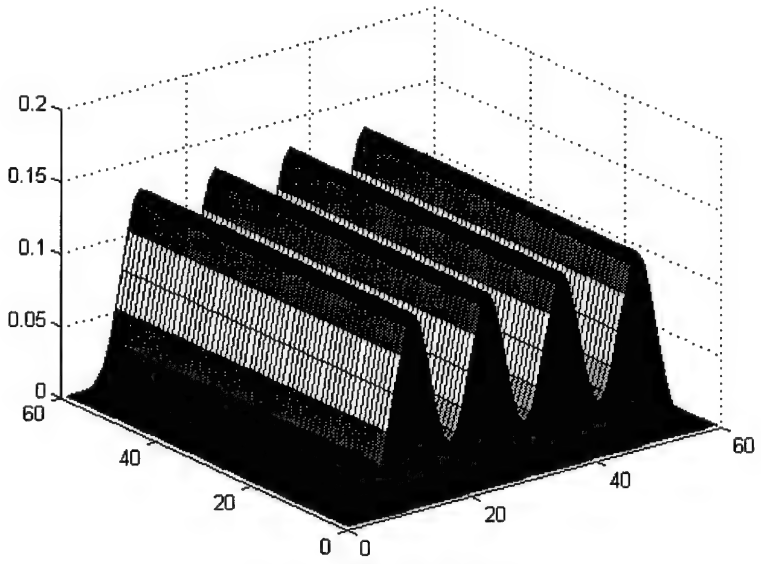

Figure 16. Sea Waves

The same test that was performed on the random surfaces was applied to the surface shown in Figure 18. The results are as follows:

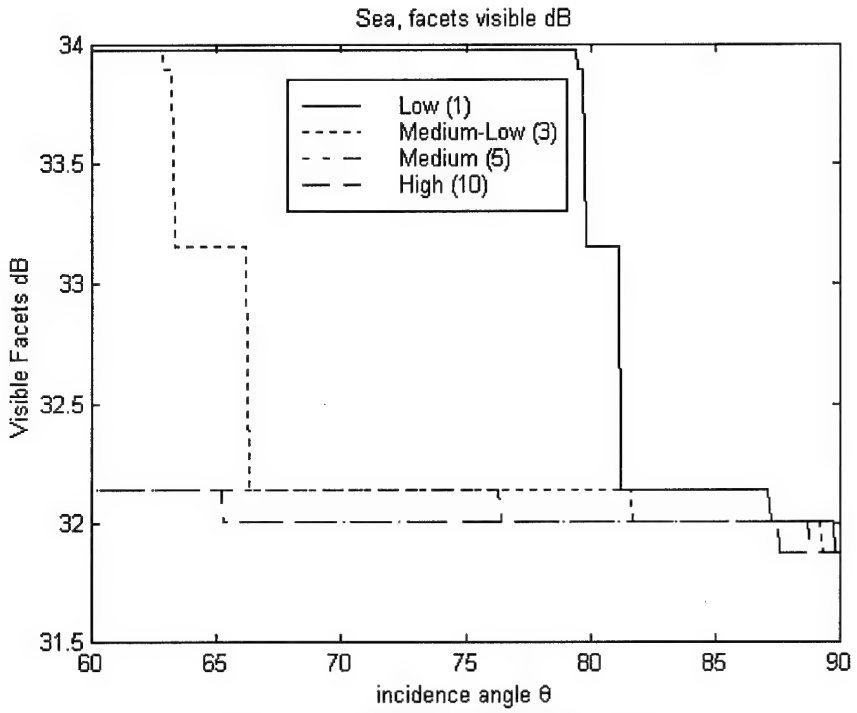

Figure 17. Visible Facets in dB (Sea)

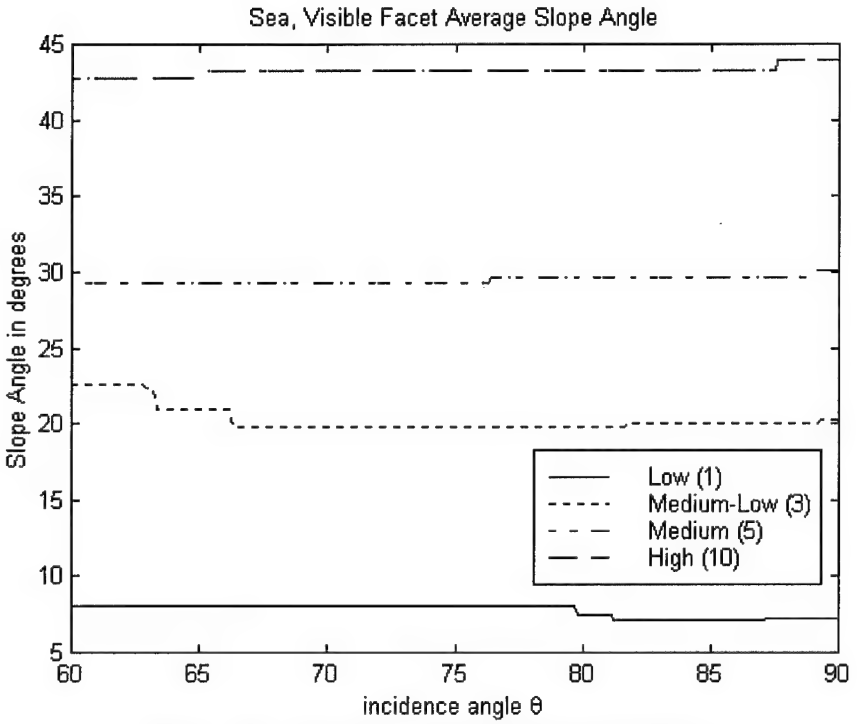

Figure 18. Average Visible Facet Slope Angle (Sea)

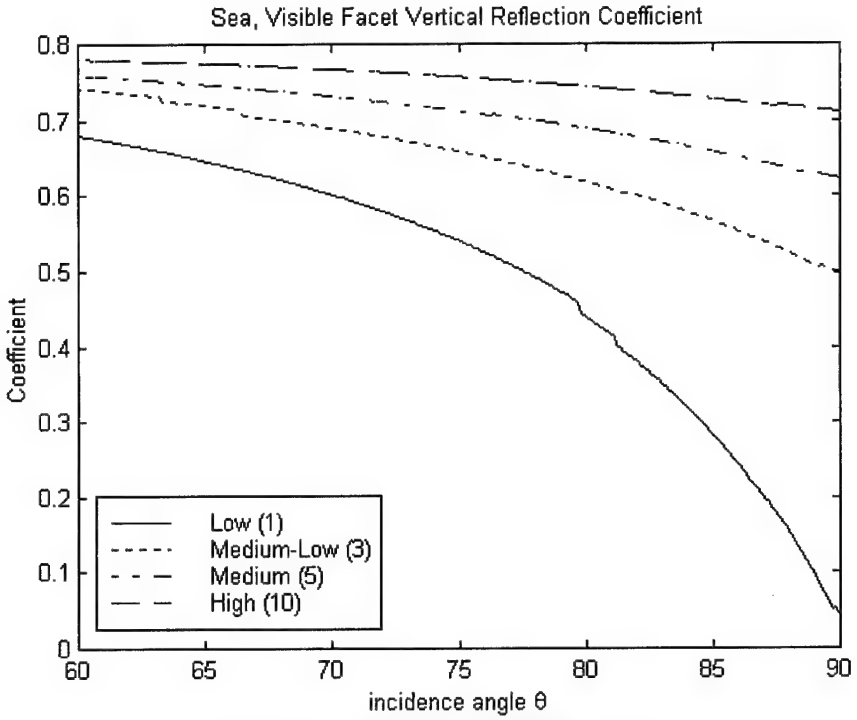

Figure 19. Vertical Coefficient (Sea)

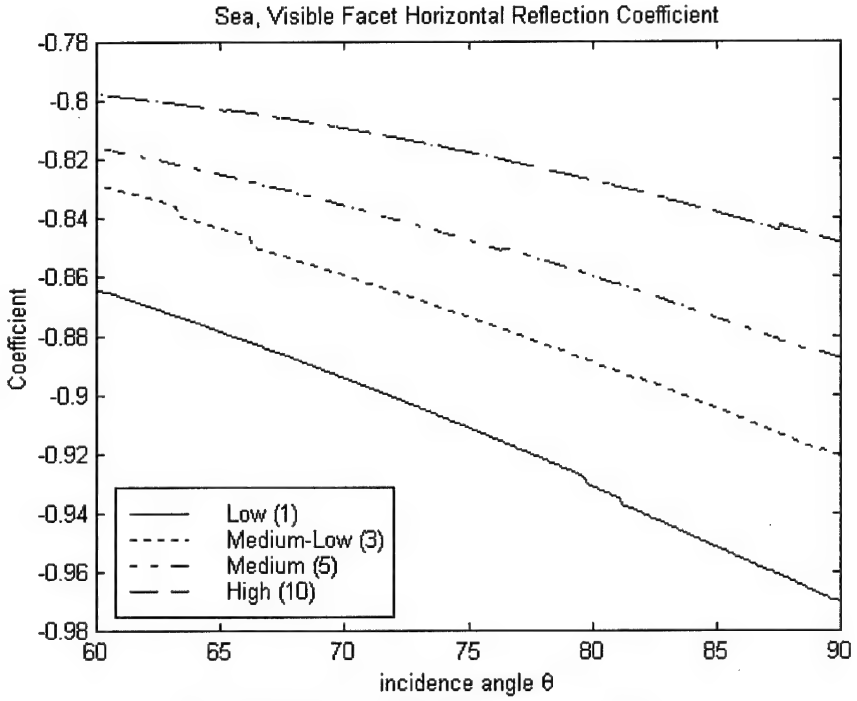

Figure 20. Horizontal Coefficient (Sea)

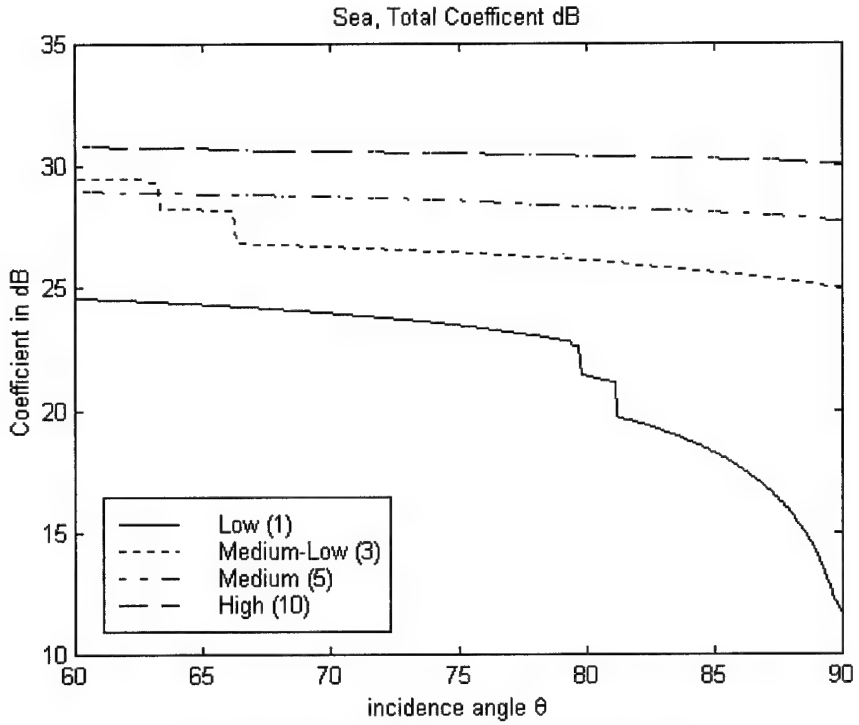

Figure 21. Total Coefficient in dB (Sea)

The sudden spikes in the graphs of facets visible and total "σ^{o}" are due to the surface model shape. On each wave, there are lines of facets that will become visible at certain viewing angles. Since the surface has ten waves, if a viewing angle is passed, 10 times the number of facets will become visible and spike the line. This modeling method does not affect the overall data or its conclusion.

	Low	Low-Medium	Medium	High
Δ% Visible Facets	62.3 %	62.3 %	6.2 %	6.2 %
Δ% Ave. Slope	1.1 %	3.1 %	0.9 %	1.2 %
Δ% Vert. Coeff. max mag. (0.79)	45.2 %	24.5 %	13.7 %	7.0 %
Δ% Hori. Coeff. max mag. (-0.79)	10.6 %	9.2 %	7.1 %	5.0 %
Δ% Total	94.8 %	65.1 %	24.7 %	15.2 %

Table 3. Δ% Change in factors (Sea)

Again, since the % change is largest in the visible facets, for all four surface heights, this shows that the number of scatters is the dominant affect on σ^o.

All three simulated surfaces (grass, trees, and sea) have shown the same effects of number of facets vs the average slope and Fresnel coefficients on "σ^o". This implies that a model that works on sea surface "σ^o" could be used in a land environment. RADLAB noticed a similar roughness effect and that will be discussed next.

2.4.6 RADLAB Sensitivity to Roughness and Moisture Content.

RADLAB, at the University of Michigan modeled the effect of surface roughness on measured data and compared them to the effect made by moisture content. By using a soil dielectric model given in Appendix E of Ulaby et al. [1], they measured the change in σ^o based on moisture to be about 5.5 dB at 10 GHz and less than 3 dB at 95 GHz. This was over the incidence angle range $55^o \leq \theta \leq 85^o$ [7]. This implied that most of the variation exhibited by σ^o in the shadow region would be due to surface roughness since σ^o changed by a much greater dB amount over the angle range.

To better show this effect, RADLAB calculated a roughness factor for 6 surfaces they had data at 95 GHz [7]. Roughness was calculated by:

$$\text{Roughness} = k \cdot s \tag{17}$$

where $k = 2\pi/\lambda$ (wave number) and s is the rms height (Standard Deviation). The smaller the ks is, the smoother the surface. They plotted σ^o, both measured data and theoretically calculated curves, for two types of surfaces, smooth surfaces ($ks < 2$) and rough surfaces ($ks > 5$) [7]. The next two figures show the results.

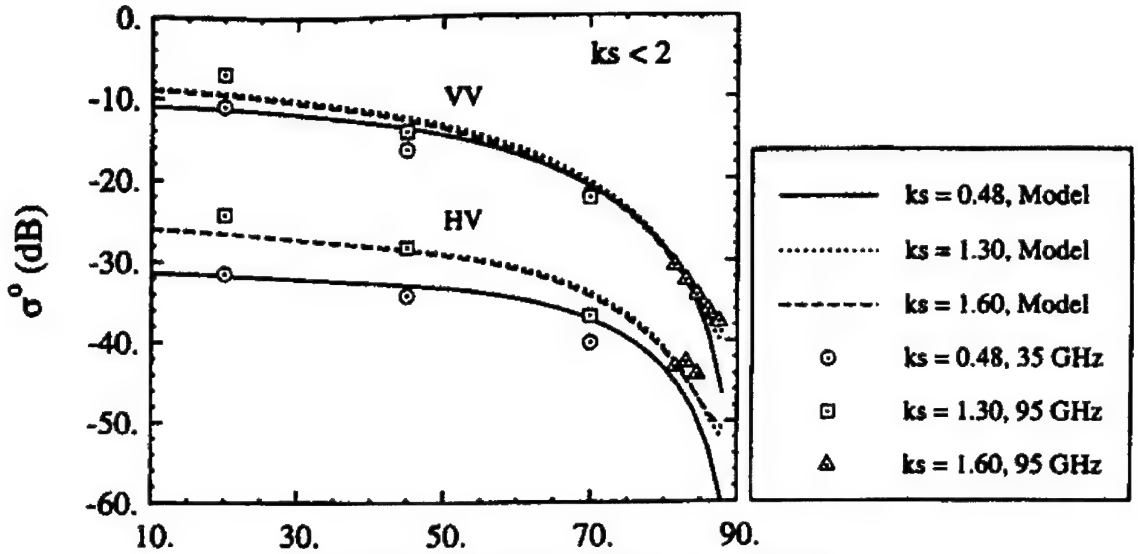

Figure 22. Measured values of VV and HV coefficients for ks < 2 [7]

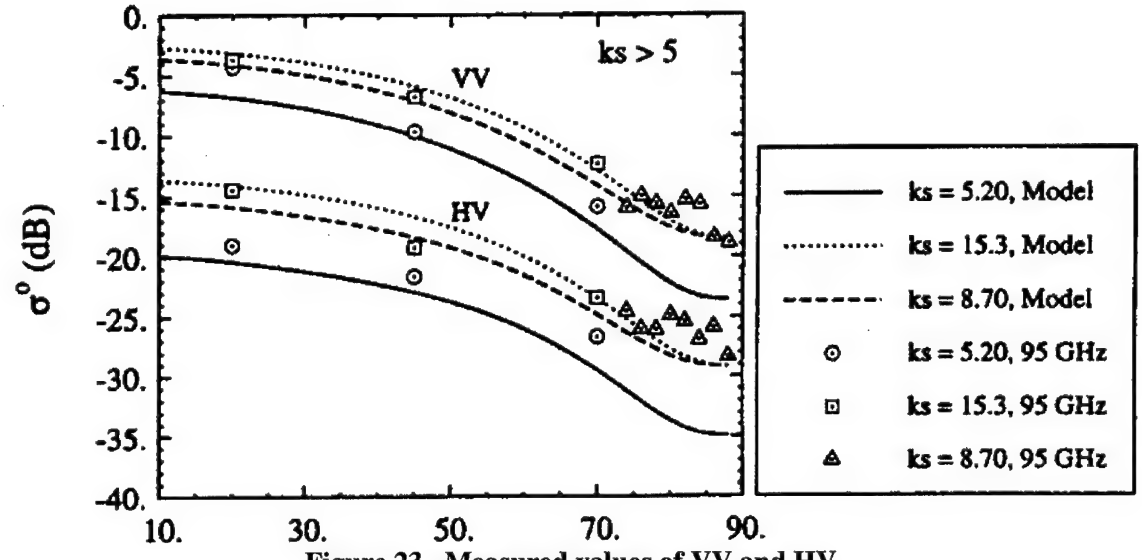

Figure 23. Measured values of VV and HV coefficients for ks > 5 [7]

For smooth surfaces with ks < 2, σ^o decreases at a steep slope up to 88° (the maximum measured data angle). In contrast, for rough surfaces where ks > 5, shows a gentle slope relative to the incidence angle. Both graphs show the need for a curve generator that produces shallow slope curves for very rough surfaces.

Because the three previous total σ graphs (random grass, random trees, and water waves) exhibit the proper low-grazing curves, they imply that surface roughness is the primary source of change in σ^o in the shadow region. All that would be left is to set the overall value or "height" of the curves such that the generator will return the correct σ^o. σ_{WM} **GEN** can provide such "height". A low-grazing sea model for use in curve generation is discussed in chapter 3.

Now, we will discuss the only available low-grazing data and then discuss two other low-grazing terrain models that were considered, but finally rejected.

2.5 Analysis of Available Grazing Data

The only available data for grazing angles above 80^o was from the Army Research Laboratory (ARL). It was measured in support of the Longbow radar program from 1995-96. They used a pulse radar, measuring at 95 GHz (W-band), with an effective 1^o beamwidth. The incidence angles varied from 85^o to 89^o with most of the data measured near 85^o [6].

Because only the mean and standard deviation of the measured data were available, the incidence angle is assumed to be 85^o. Some data was measured closer to the horizon and could induce errors in the published data. I assumed that the data measured closer to the horizon did not deviate from the 85^o data and would not affect the published mean and standard deviation [6].

Another possible source of error in the published data is snow on the test surfaces. During measurements of woods and plains-type terrain surfaces, snowfall covered some of the test areas. While the snow depth was measured and published, the areas that were

covered while measured and the areas that weren't covered was not indicated in the ARL report. Since the number of snow covered measurements was minimal, I assumed the published data was not greatly affected and did not need modification.

A number of surfaces were measured by the Army. However, the only surfaces that equate to available data from RADLAB were grasses, trees, and bushes (short vegetation). Some of the trees and grasses data was taken with snow on the measured cell. As stated before, this did not affect the use of the published data. However, it must be noted that RADLAB has separate measurements for snow [6].

Terrain Cell Type (RADLAB Designator)	VV Polarization
Trees (Coniferous) (B)	mean (-17.6) SD (1.0)
Trees (Deciduous) (B)	mean(-16.4) SD(2.3)
Grass (C)	mean(-18.3) SD(1.7)
Short Vegetation (E)	mean(-19.3) SD(1.9)

Table 4. ARL measured data, Mean σ^o and Standard Deviation in dB

2.6 Currently Available Low-Grazing Terrain Backscatter Models

In researching backscatter, two land clutter models, besides the squared cos term mentioned in Chapter 1, were repeatedly discussed. Georgia Tech and RADLAB at UM developed deterministic models to fit their available data. While neither model was used in the final solution or for validation, a discussion of both models is included for comparison to the final developed model.

Both models suffer from two common problems. The first, and more serious, problem relates to their deterministic properties. Both models return a mean for the terrain constants they have. However, neither model generates data with the randomness of

nature. The second problem depends on their ability to accept new measured data. Since both models are curve-fitting algorithms, any new measured data would require more curve-fitting analysis before the data could be used

2.6.1 Georgia Tech Land Model.

Because of the difficulty in modeling a complex terrain surface, personnel at Georgia Tech created an empirical model. Instead of measuring the effects of surface roughness, surface composition (moisture content), distribution of scatterers, and other factors, the model was fitted to a selected subset of available data [3].

$$\sigma^{o} = A(\theta + C)^{B} \exp\left[-D \Big/ \left(1 + \frac{\sigma_h}{\lambda}\right)\right] \tag{18}$$

A, B, C, & D are derived constants based on fitting the curve to the measured data, not the measured frequency, surface type and roughness, or other effects. σ_h is the standard deviation of the surface in decimeters and λ is the beam wavelength.

While there are available constants for almost all of the nine terrain surfaces, the Georgia Tech model does not have the frequency range (only in Ka and W-band) and angle range ($35^{o} \leq \theta \leq 70^{o}$) that is desired. Also, in comparison to the sea curves, the land model does not drop near the horizon as usually seen in data (see Figure 24).

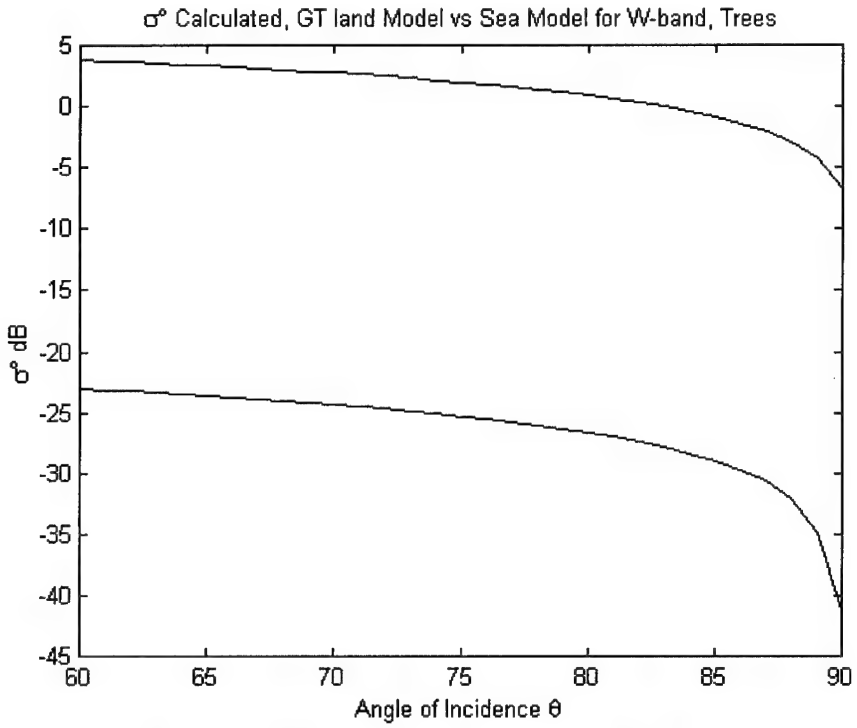

Figure 24. Georgia Tech Land Model vs. Sea Clutter Model, GT Curve (Top), Sea Clutter Model (Bottom)

Since the Georgia Tech model was developed for "plateau" region operations ($35^\circ < \theta < 70^\circ$), its shadow region operations are limited at best (as seen in Figure 24). It is for this reason that this model was not considered for final usage with σ_{WM} **GEN** .

2.6.2 RADLAB Model.

Personnel at the University of Michigan base this model on the extensive collection of correlated measured data [1]. Like the Georgia Tech model, the RADLAB model is fitted to a selected subset of measured data. The RADLAB model contains two equations: a mean σ° equation and a standard deviation equation based on the measured data. The idea is that a more random σ° could be generated using these two equations.

$$\sigma^{o}_{mean}(dB) = P_1 + P_2 \exp(-P_3\theta) + P_4 \cos(P_5\theta + P_6) \quad (19)$$

$$SD(\theta) = M_1 + M_2 \exp(-M_3\theta) \quad (20)$$

where P_x and M_x are frequency and terrain dependent constants.

While this model and σ_{WM} **GEN** are based on the same collection of data, the RADLAB model is more limited than σ_{WM} **GEN** in the frequencies and terrain types that are available. This limitation, as well as RADLAB's inability to accept new data without curve-fitting, made the RADLAB model less desirable to use.

2.7 Summary

The overall problem of measuring and simulating σ^{o} for terrain was shown. The measurements of the faceted random and sea surfaces appear to suggest the theory that at low-grazing angles, most of the effect on σ^{o} is due to the overall surface roughness, not surface composition. This allows for a low-grazing sea model to be use to model terrain clutter. The ARL data was analyzed and discussed for possible errors. It was decided that the potential errors would have very little effect on the final product and could be safely disregarded. Finally, two currently used land models were compared and rejected due to their operational limits.

III. Methodology

3.1 Introduction

The simulated surface example, set forth in section 2.4, allows for the usage of a σ^o generator of a surface to be used with a surface with a similar roughness. All that would be needed to be determined would be the overall value of the curve. σ_{WM} **GEN** completes this task.

As seen in the last chapter, there are very few terrain models available, and of those, none have the frequency range, terrain mixture, and angle set that is needed. However, there are two sea clutter σ^o models, Georgia Tech and the Center of Naval Analysis (CNA), which contain the angle set and dependence on wave height (surface roughness) that is desired [5]. Because the Georgia Tech model had the largest available frequency range, it is the selected model and used in the final generator.

This chapter will discuss the development of the Georgia Tech model and describe how it is integrated with σ_{WM} **GEN**. Then the completed model will be compared to Army data in four cases where the Army data coincides with the RADLAB data (basis for σ_{WM} **GEN**).

3.2 Sea Model Theory

The model theory is based on Currie's description of the millimeter portion ($\nu > 30$ GHz) [3]. The original model was developed and described by Horst and Perry, however the original document is not available [15]. The greater than millimeter wave portion ($\nu < 30$ GHz) was derived from the ALARM 91 model from SAIC [5].

Symbol	Definition
θ	Incidence angle
λ	Radar wavelength
ϕ	angle between boresight and wind direction
V_{wind}	Velocity of wind (m/s)
HH or VV	Polarization of transmitted and received waves

Table 5. Input parameters for Sea Clutter Model

Symbol	Definition	Variable Dependence
h_{wave}	Wave height	V_{wind}
r	roughness parameter	λ, ϕ, h_{wave}
A_I	multipath interference factor	r
A_u	upwind-downwind factor	ϕ, θ, λ, u_x
u_1, u_2, u_3	est. parameters based on meas. data	
A_w	Wind speed factor	V_{wind}, qw
qw	power factor	λ, qw_1
qw_1	est. parameter based on meas. data	
σ^0_{xx}	calculated backscatter for HH or VV	λ, θ, A_i, A_u, A_w, c_x, z_x
c_1, c_2, z_1, z_2, z_3, z_4, z_5, z_6	est. parameters based on meas. data	

Table 6. Internal variables for Sea Clutter Model and dependence

The problem of developing a model for sea backscatter is a complicated one at best, since it is dependent upon radar frequency, sea state, incidence angle, wind/sea direction,

polarization, and other factors. Georgia Tech researchers designed an analytical model to describe sea clutter backscatter using empirical constants derived from measured data [3].

The clutter model calculates σ^o as the product of three variables: multipath interference, sea direction, and wind speed. Each of these factors is, in turn, a function of the appropriate variables.

The multipath interference effect factor, between the direct and scattered fields from the surface for horizontal polarization, is derived from forward scatter theory assuming a Gaussian distribution of surface height with a standard deviation of σ^o_{HH}

A roughness parameter, r, is defined to be:

$$r = (14.4\lambda + 5.5)\frac{\theta \cdot h_{wave}}{\lambda} \tag{21}$$

where

$$h_{wave} = 0.348\left(\frac{V_{wind}}{11}\right)^{1.8} \tag{22}$$

The average wave height (h_{wave}) is defined to match the sea-state descriptors as set in Skolnik [9, p136].

Sea State	Wind Speed (m/s)	Wave Height (m)
1 (smooth)	< 3.5	< 0.3
2 (slight)	3.5 – 6.2	0.3 – 0.9
3 (moderate)	6.2 – 8.2	0.9 – 1.5
4 (rough)	8.2 – 9.8	1.5 – 2.4
5 (very rough)	9.8 – 11.8	2.4 – 3.7
6 (high)	11.8 – 15.4	3.7 – 6
7 (very high)	15.4 - 23.2	6 – 12.2

Table 7. Sea-State Surface Descriptors (Numbers are not integer values due to wind speed set in knots and wave height set in feet.)

For this model, the sea states do not need to be integer values. A sea can be described to be 3.5 if the wind speed and wave height match for that particular sea state. In the final integrated model, a number of surfaces are assigned non-integer sea-states for roughness parameters. More information can be found in Chapter 4.

The interference term A_i is given by

$$A_i = \frac{r^4}{1+r^4} \tag{23}$$

The behavior of σ^o versus incidence angle falls into two distinct regions: a low grazing angle region in which σ^o is a strong function of angle, and a plateau region in which σ^o is approximately independent of the angle. Due to this, only σ^o data from the plateau region was used in determining the parametric dependencies for the model.

The sea direction term is based on upwind-downwind data, although the reference for the aspect angle ϕ should be the sea wave propagation vector rather than the wind vector. The up-down data is dependent on incidence angle θ, increasing as θ approaches the horizon, but approaching a finite value at horizon [3]. Since there is insufficient data to determine clearly the functional form of the dependence, a simple function, cos ϕ, is chosen, where ϕ is the angle between antenna boresight and the upwind direction [3]. For system simplicity, ϕ is fixed at 90°, but can be changed if necessary. The upwind-downwind interference term A_u is defined to be:

$$A_u = \exp[u_1 \cos\phi(1-2.8\theta)(\lambda+u_2)^{u_3}] \tag{24}$$

Currie states that the dependence of σ^o on the sea state has been shown to be more a function of wind speed than of wave height [3]. This is interesting because the wave height

(h_{wave}) is calculated from the wind speed. For simplicity, the wind speed term, A_w, is defined as:

$$A_w = \frac{1.94 V_{wind}}{\left(1 + \frac{V_{wind}}{15}\right)^{qw}} \tag{25}$$

$$qw = qw_1(\lambda + 0.2)^{-0.4} \tag{26}$$

Through curve fitting of the available measured data, the final σ^o equation was found to be:

$$\sigma^o_{HH} = c_1 \lambda \theta^{c_2} A_i A_w A_u \ (\nu \leq 10 \text{ GHz}) \tag{27}$$

and

$$\sigma^o_{HH} = c_1 \theta^{c_2} A_i A_w A_u \ (\nu > 10 \text{ GHz}) \tag{28}$$

The correction factor for vertical polarization has been found to be a linear fit compared to the σ^o for horizontal polarization. Using the data, σ^o_{vv} is:

$$\sigma^o_{VV} = \sigma^o_{HH} - (h_{wave} + z_1)^{z_2} (\theta + z_3)^{z_4} \lambda^{z_5} 10^{z_6} \tag{29}$$

where c_x and z_x are empirically derived frequency constants.

Cross polarization (σ^o_{hv} & σ^o_{vh}) data was not available when the model was developed. Ulaby et al. have found that near the horizon, measured σ^o_{vv}, σ^o_{hv}, & σ^o_{vh} are within 2.0-4.0 dB of each other with cross-polarization usually less than linear-polarization [7]. The final model will use σ^o_{vv} curves for the cross-polarizations.

The final result of this model are sea clutter curves as shown in the next figure. As the sea surface becomes rougher, the curve shape flattens and does not drop off until very

close to the horizon. This effect has been shown in measured data [4, 7] and is the desired behavior for the final integrated model.

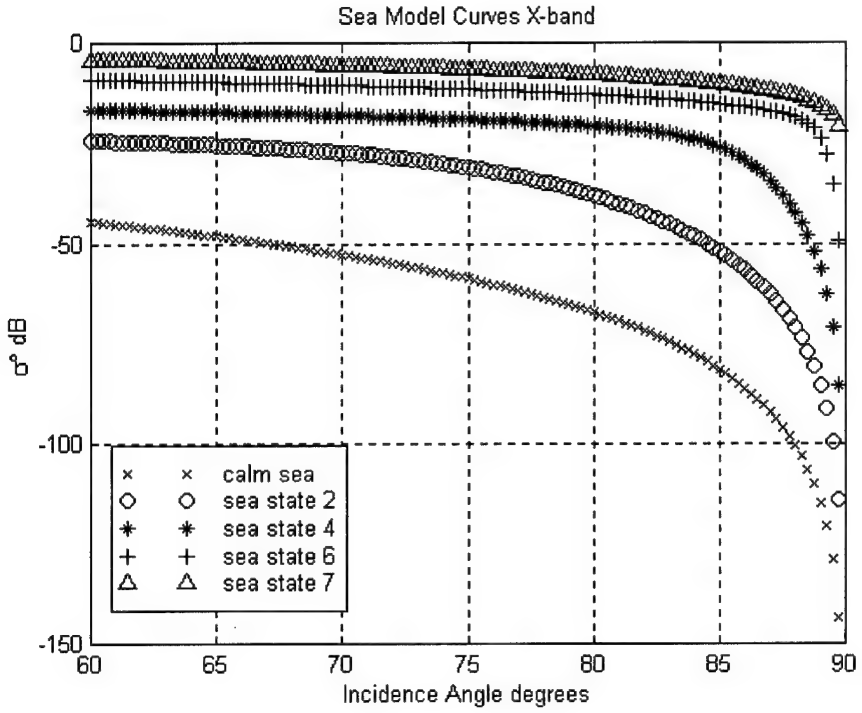

Figure 25 Sea Model Curves for 5 Different Sea States

In the final integrated model, an "elbow" effect will occur shortly after the integration point between the measured data and the sea curves. This is due to the final dropping off of the sea model. Validation tests in section 3.5 will show that the "elbow" effect has no adverse consequences on the final model results.

3.3 Wilson/Mediavilla Model

The following equation is the basis behind σ_{WM} **GEN**:

$$\sigma = \beta \cdot \left(-\ln(U)^{\alpha}\right) + \gamma \tag{30}$$

The α–β–γ combinations are set such that they would yield the required mean σ^o and SD(θ) values given by the RADLAB data. A typical set of values would be of the form:

$$\alpha = 0.06, 0.061, 0.062, \ldots, 2.0 \tag{31a}$$

$$\beta = 0.01, 0.011, 0.012, 0.013, \ldots, 14.0 \tag{31b}$$

$$\gamma = 0.01 \tag{31c}$$

When a combination of α, β, and γ generates the mean σ^o and SD(θ) for a given surface and angle, those values of α, β, and γ are placed in a lookup table. When a σ^o is requested, the model retrieves the necessary α, β, and γ and combines them with a U(0,1) randomly generated number. The method of generating α, β, and γ for a given terrain and angle is described in [2] and the reader is invited that work for more information. For this system, the model is representative of real terrain scattering σ^o measurements for $0^o \leq \theta \leq 80^o$.

3.4 Model Integration

Since σ_{WM} **GEN** is based on measured data, the integrated model will return the σ_{WM} **GEN** σ^o whenever possible. The sea model is only implemented when the requested angle is unavailable through σ_{WM} **GEN**.

If such an angle is requested, the system inquires σ_{WM} **GEN** for the highest measured data incidence angle. σ^{o}'s values are calculated for the highest angle, and 1^{o} and 2^{o} below the highest angle. These values are averaged to create an artificial "plateau" for the sea model to start calculations. This plateau is usually calculated around $\theta = 75^{o}$ for most terrain types and frequency bands.

This method of plateau calculation combines the probabilistic nature of σ_{WM} **GEN** with the accuracy and stability that comes from averaging a set of points [2, 13]. All previous near-horizon models provide the same answer for a given terrain type and frequency band. By using σ_{WM} **GEN**, the probabilistic nature of is harnessed while the sea model gains a stable point to start from.

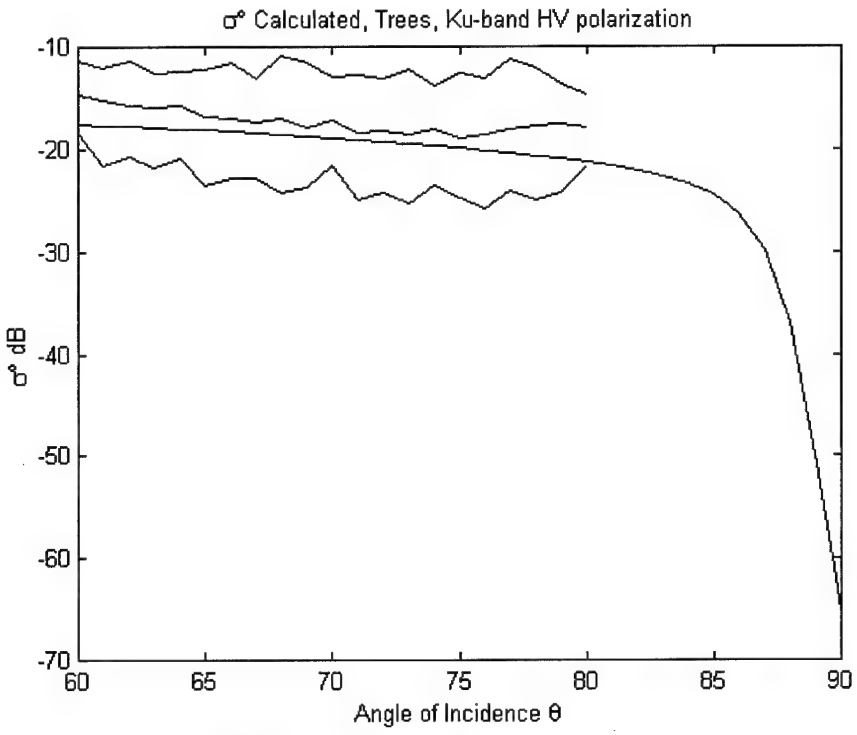

Figure 26. Trees, Ku-Band, Before averaging to plateau

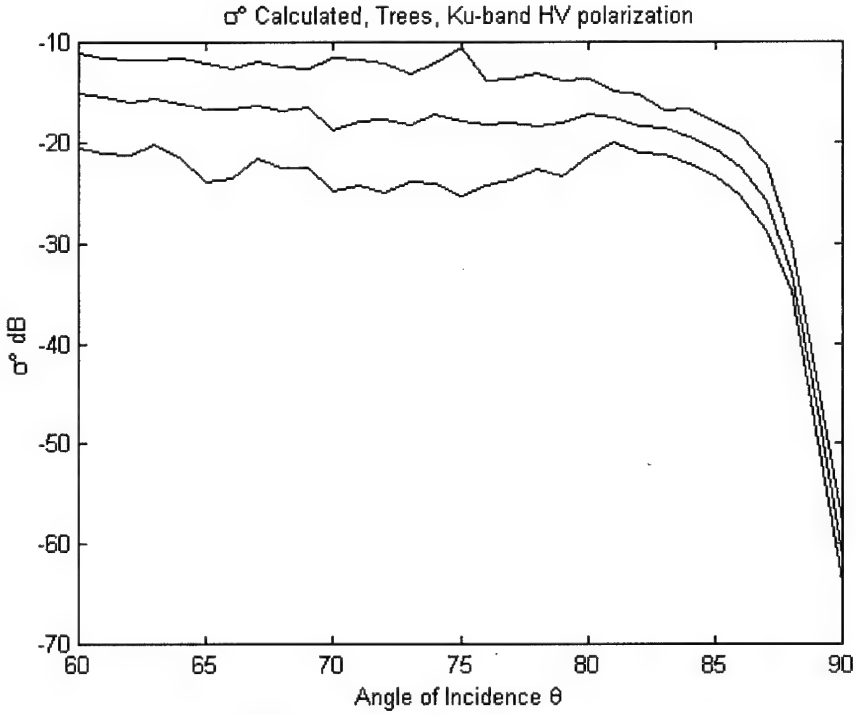

Figure 27. Trees, Ku-Band, After averaging to plateau

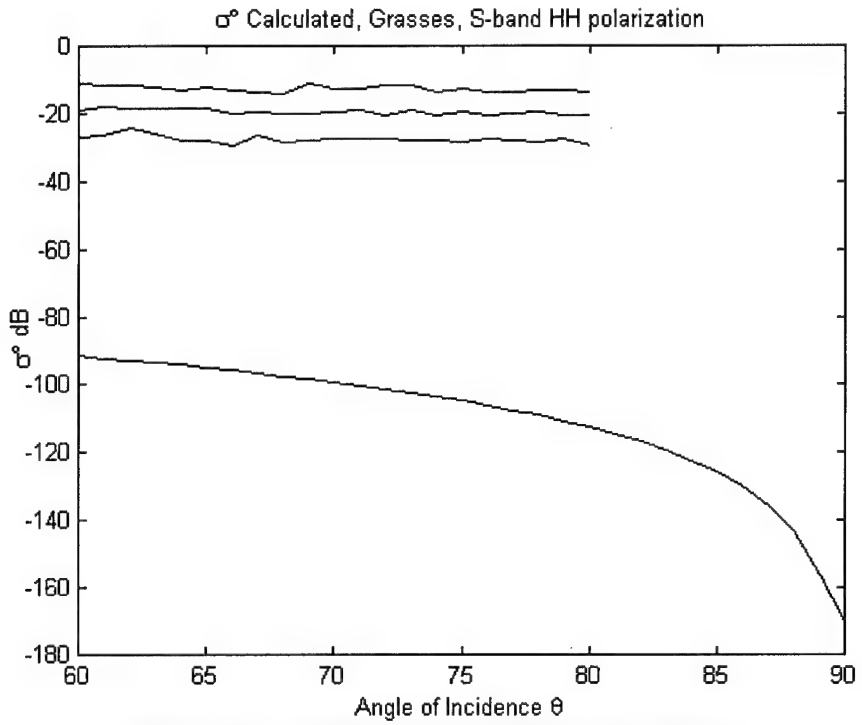

Figure 28. Grasses, S-Band, Before averaging to plateau

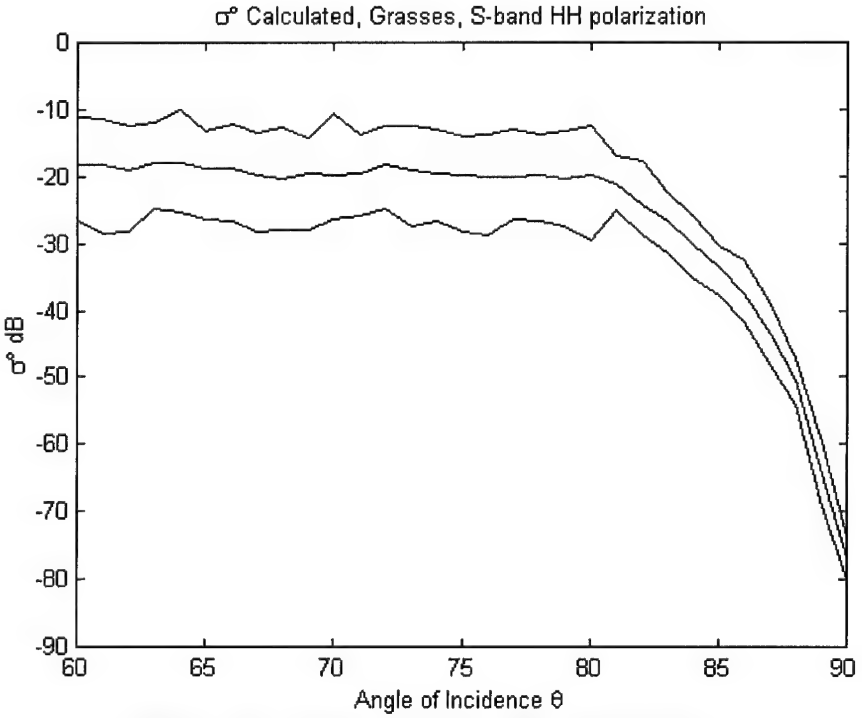

Figure 29. Grasses, S-Band, After averaging to plateau

The probabilistic properties of σ_{WM} **GEN** pass though the sea model to affect any low-grazing angle calculated σ^o. This property is shown in the four validation figures in the next section.

3.5 Model Validation

Since the Army data was measured in W-band, only four terrain types match to RADLAB data. These terrain types are grasses, vertical-vertical; coniferous trees (evergreens), vertical-vertical; deciduous trees (with leaves), vertical-vertical; and short vegetation, vertical-vertical.

The single vertical line at 85^o is the range of the Army data out to one standard deviation. The two lines running outside of the centerline (the mean σ^o) are the minimum and maximum σ^o's calculated by the final integrated model.

As mentioned before in section 3.2, each figure shows an "elbow" effect at some point after the merger point from measured data to sea curve (around $\theta = 80^o$). That is, the resulting curve drops faster than it did at lower angles. The following figures show this effect resulting in the final model matching the measured data. This is most noticeable in Figure 33 (Short Vegetation) where the ARL measured data line ($\theta = 85^o$) is lower than the RADLAB measured data ($\theta \leq 80^o$).

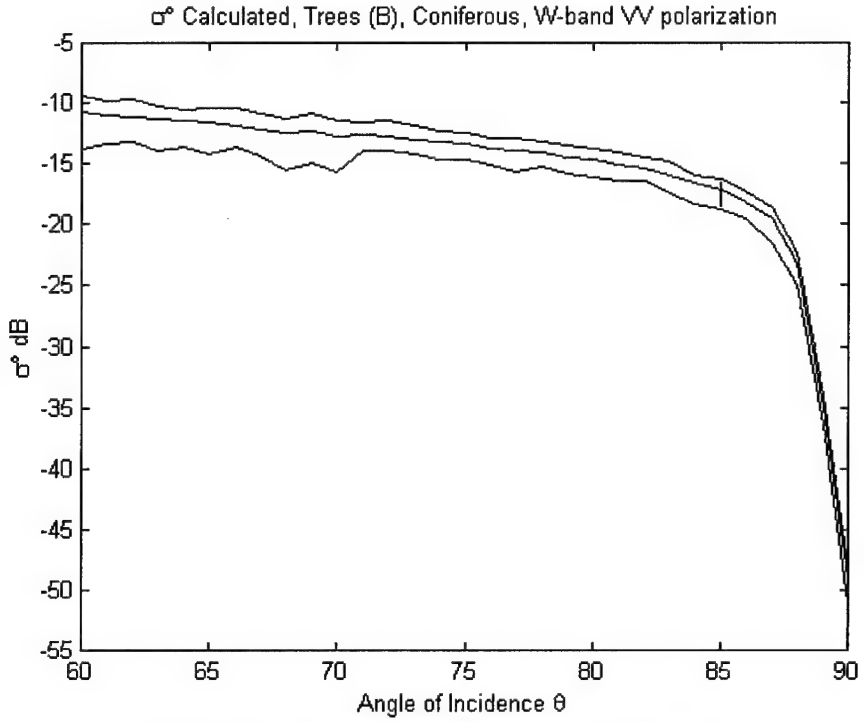

Figure 30. Comparison of the final model with ARL data (Trees Coniferous, W-Band, VV-polarization)

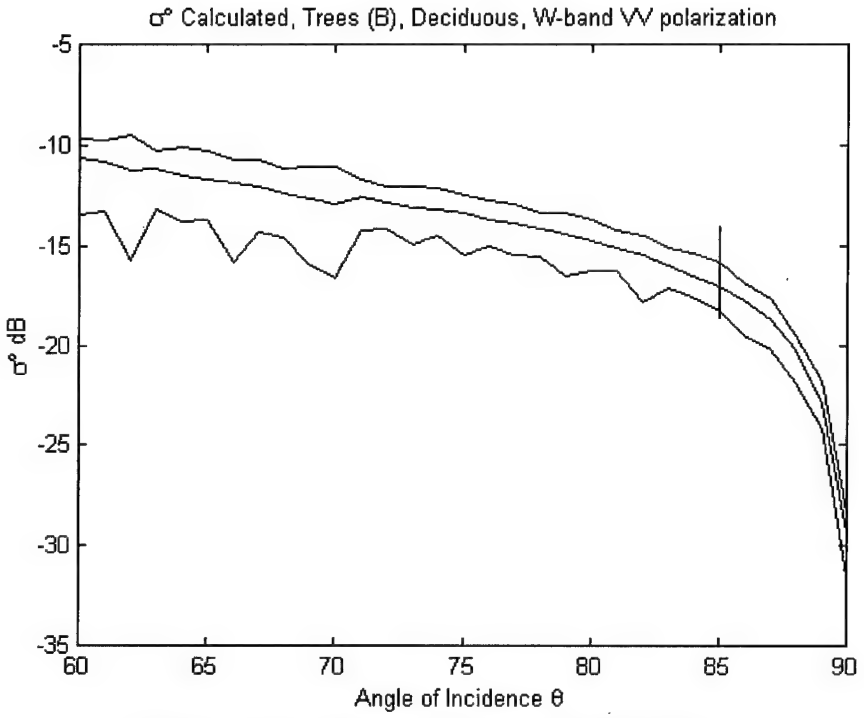

Figure 31. Comparison of the final model with ARL data (Trees Deciduous, W-band, VV-polarization)

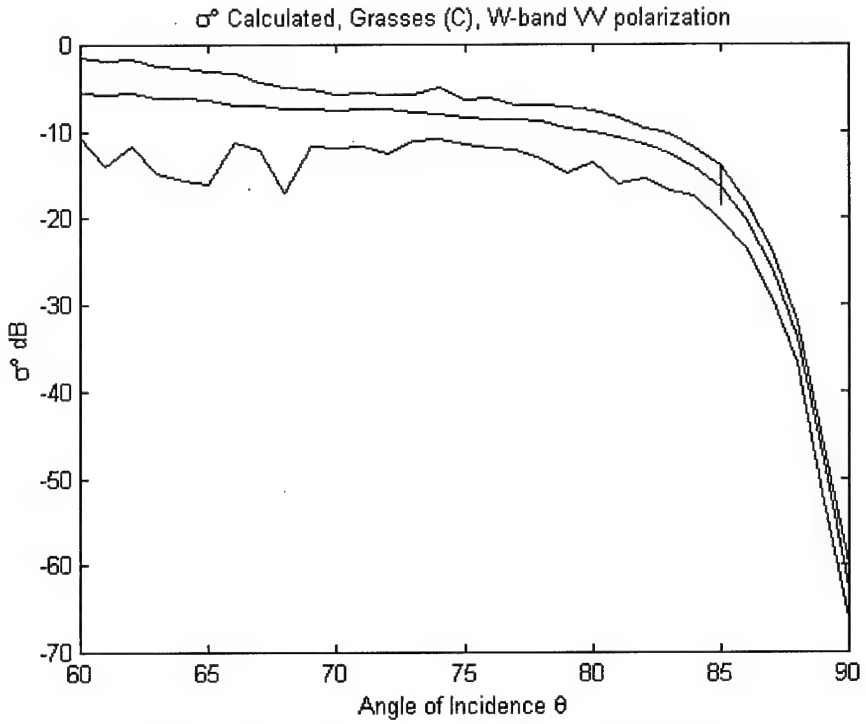

Figure 32. Comparison of the final model with ARL data (Grasses, W-Band, VV-polarization)

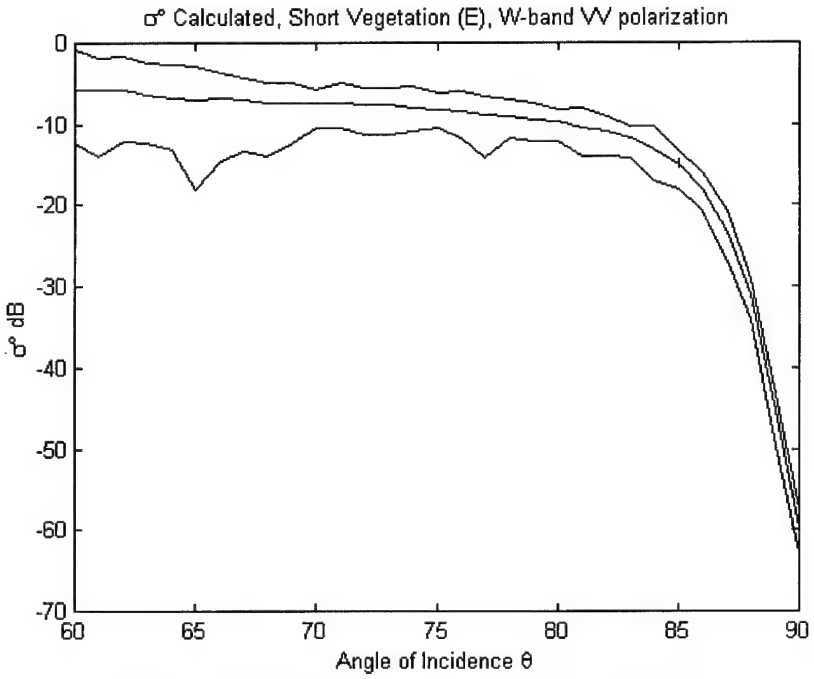

Figure 33. Comparison of the final model with ARL data (Short Vegetation, W-band, VV-polarization)

With the exception of short vegetation, the final model σ^o mean, maximum, and minimum are within, or very near, the first moment of the measured data. The disconnect of min/max of the final model for short vegetation to the first moment is due to the apparent small sample size of the ARL data. However, the mean of the final model matches closely to the mean of the measured data.

3.6 Summary

This chapter has discussed the operation of the sea model used and how it interfaces with σ_{WM} **GEN** to create the final system model. A brief discussion of σ_{WM} **GEN** followed and finally, validation of the final model was done with measured data from ARL. Chapter 4 has test runs of the final integrated model over all nine terrain surfaces.

IV. Results and Discussion

4.1 Overview

Due to the lack of measured data outside of the four cases used to validate the final model, any discussion is limited to how the model performs and if the different polarization cases (HH, VV, and HV) relate to each other as they do in measured scenarios.

The following chapter displays model results for each terrain type in two different frequency bands. Comments are made for each test run as to the wave height used and if the polarizations behave as theorized.

4.2 Sea State decisions

The basis for the decision of each sea-state assignment to each terrain type is very simple. Whenever measured data near the horizon was available, the sea state was chosen experimentally by trial and error. Since only three RADLAB terrain types (grasses, trees, and short vegetation) were available under the ARL data, only three sea states were determined this way. The other six terrain type sea states were determined by comparing the three experimentally determined terrain types with the other terrain types. Surfaces smoother than grass (roads and snow) were assigned smaller sea states. Surfaces rougher than trees (Urban areas) were assigned larger sea states. All other surfaces were assigned sea states in between.

After all terrain types were assigned sea states, initial graphs were created to check if the measured data had curvature that did not match with the initial sea state. If that

happened, the sea state was either slightly raised or lowered until the sea curve matched with the measured data curve.

4.3 Model Results for selected tests

Before discussing the final model results, the behavior of the polarizations needs to be recapped. Measurements performed by RADLAB in W-band grazing angle regions have shown that VV and HH polarization measurements were within 2-5 dB of each other. Meanwhile, HV polarization measurements were usually 10-15 dB below VV and HH with VH measurements equaling HV [7].

In the figures below, the model data fits the behavior that RADLAB noted in most cases. In those figures where the polarizations did not match RADLAB observations, the measured data sample size was noticeably low. Mediavilla noted that measurement cases with small sample sizes would result in erroneous results more often than surfaces with high number of sample measurements [2]. All surfaces with very low sample sizes and very large erroneous results are identified by Mediavilla and are not used in the final integrated system model.

4.2.1 Dirt & Rocks (RADLAB Surface A).

The sea state chosen for this was 0.8. This was chosen based on the grass sea state of 1.0. Since a soil and rock field is just smoother than a field of grass, this decision is justified.

In the final results, the L-band curves are smooth with the HH and VV polarizations within a few dB and the HV polarization about 10 dB lower. The Ka-band curves show a quick dropping off at 80°. The results, however are still valid.

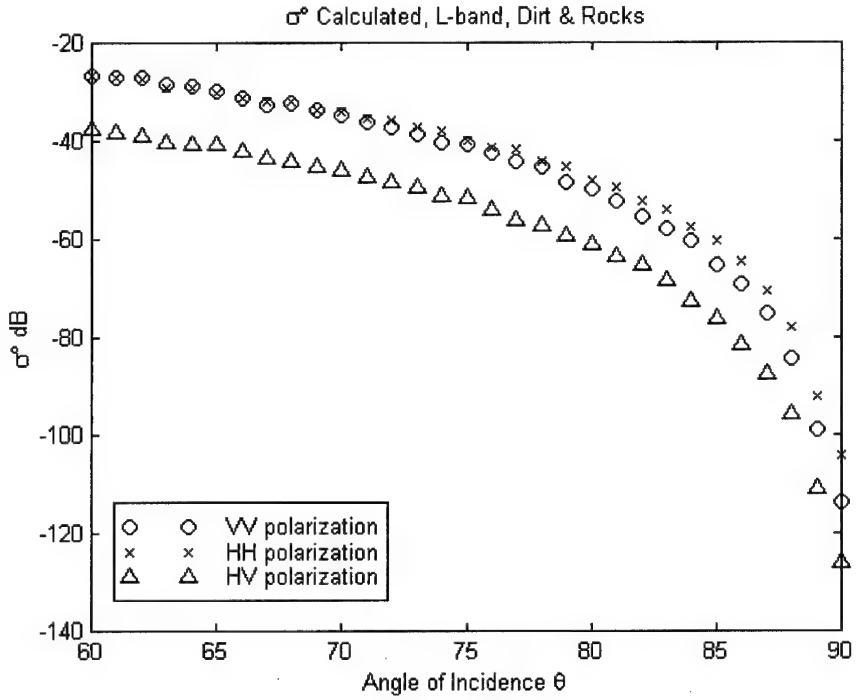

Figure 34. L-Band

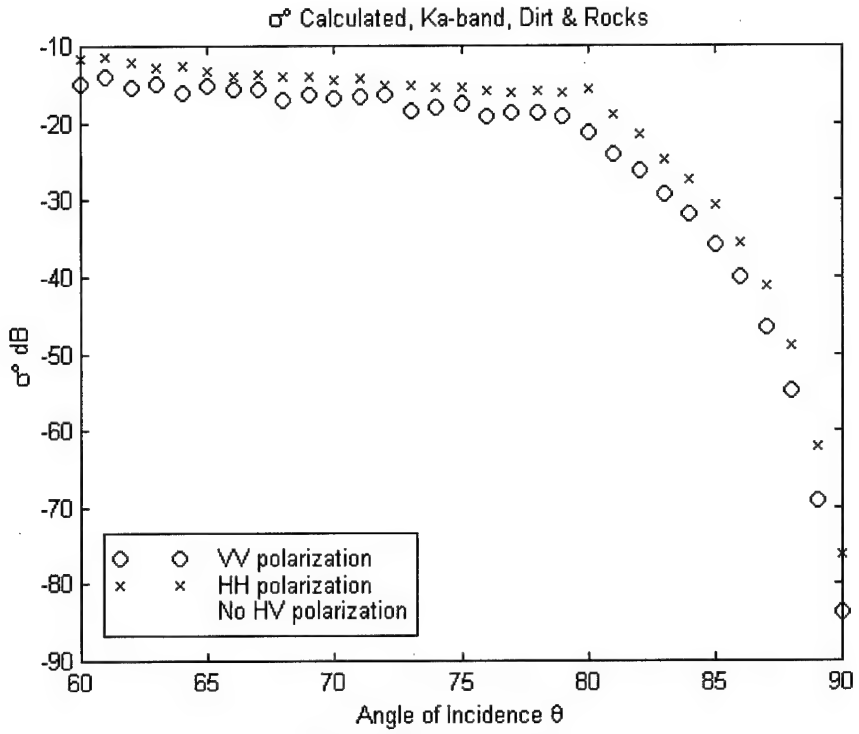

Figure 35. Ka-band

4.2.2 Trees (RADLAB Surface B).

The sea state of 3.0 is chosen for trees. This is an average of the validation results of the ARL data for deciduous and coniferous trees (sea states 4.0 and 2.0 respectifully).

For both graphs, the polarizations and curvature match very well to expectations of HH and VV above HV as well as a smooth integation and drop off. The linear and cross polarizations are not seprated by 10 dB, but this is thought to be due to the large number of vertical and horizontal reflectors (branches) present in trees.

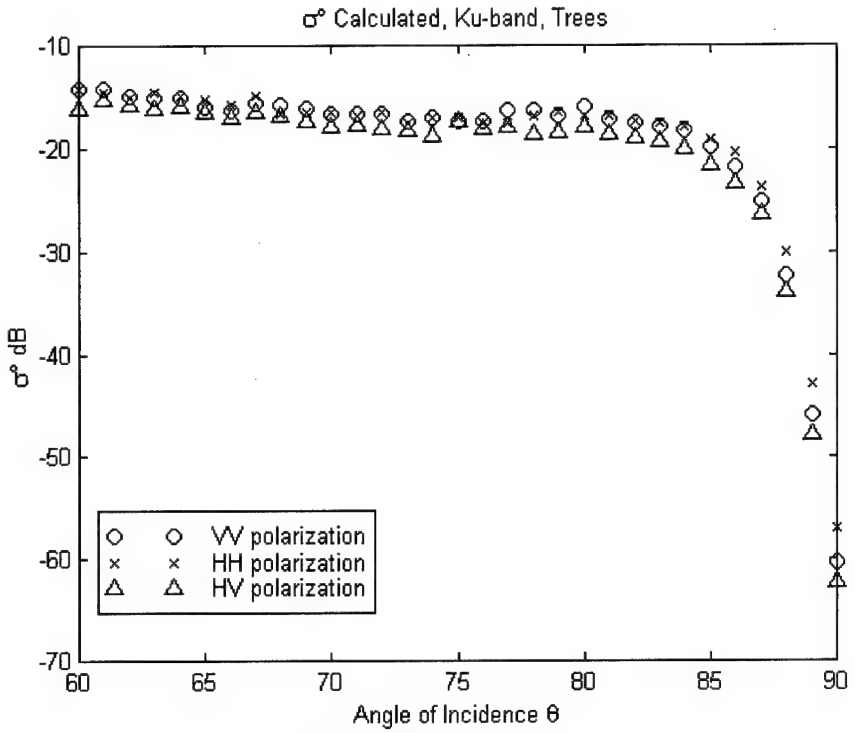

Figure 36. Ku-Band

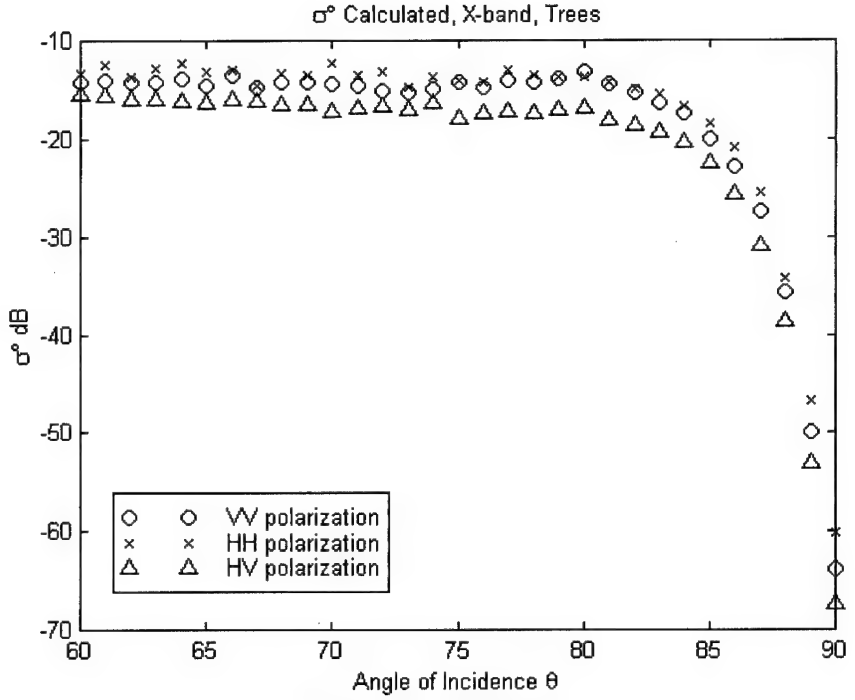

Figure 37. X-Band

4.2.3 Grasses (RADLAB Surface C).

Due to ARL data validation, the sea state of grass is set to 1.0. This does not mean that all other sea states are based off of grass; it just happened to work out.

The curvature for both graphs are mostly smooth with the exception of the linear polarizations in Figure 39. The quick drop is acceptable and not seen to be a problem.

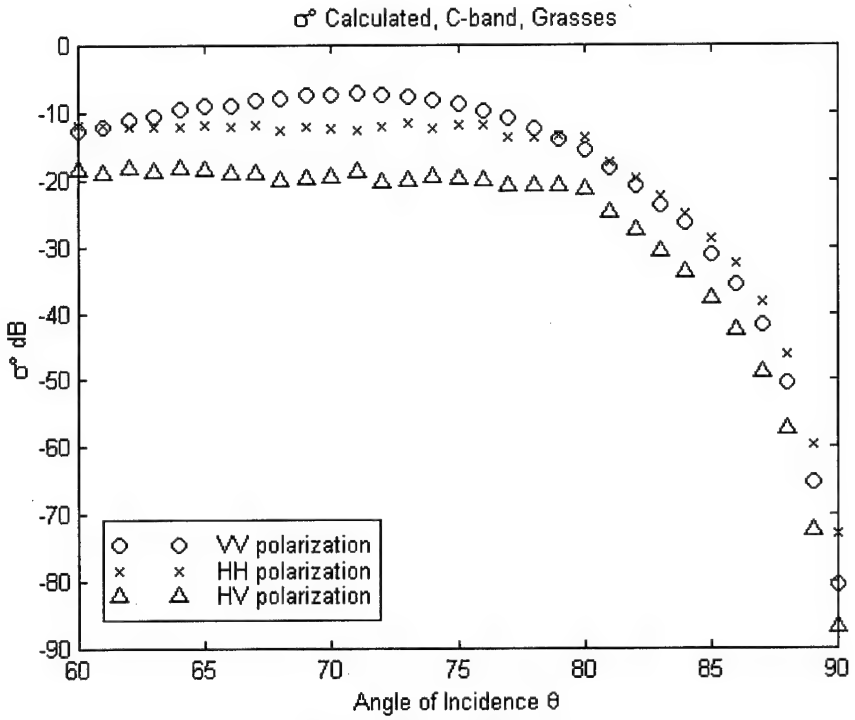

Figure 38. C-Band

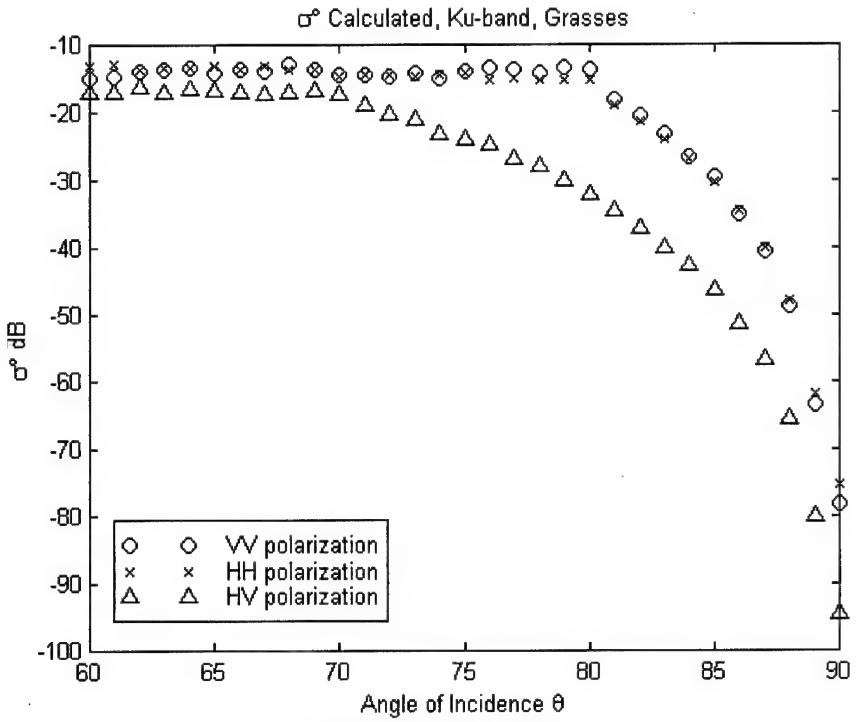

Figure 39. Ku-Band

4.2.4 Shrubs (RADLAB Surface D).

Shrubs sea state is set between short vegetation and trees at 1.7. This is because shrubs are sometimes considered short trees. The curvature is not as smooth as desired, however, it is acceptable. The polarizations behave as desired with cross ploaziation about 7-10 dB below linear polarizations.

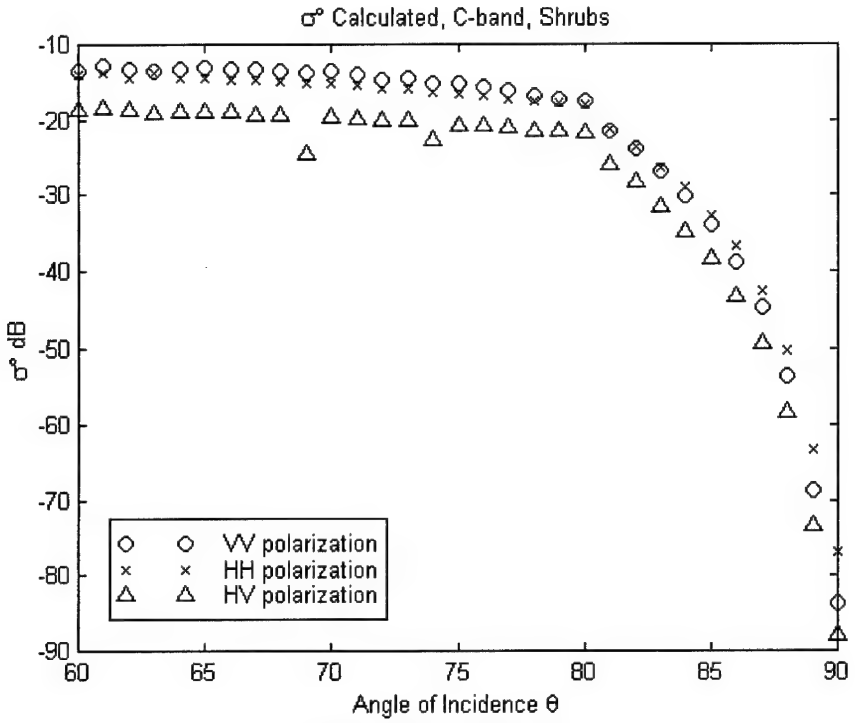

Figure 40. C-Band

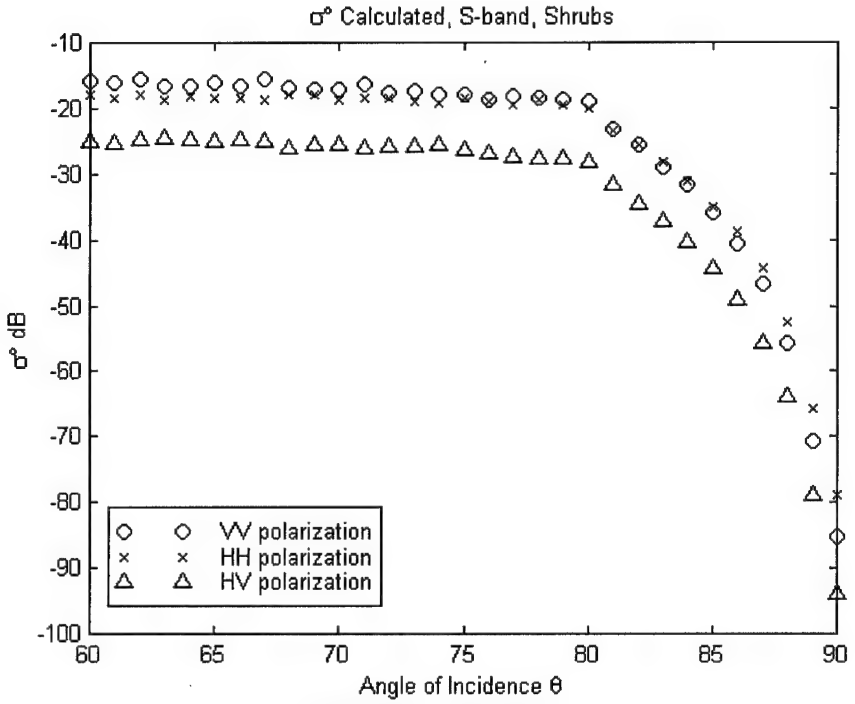

Figure 41. S-Band

4.2.5 Short Vegetation (RADLAB Surface E).

Short Vegetation is the last of the ARL data validated sea states. This sea state is set at 1.3. The curvature looks good with a small drop in Figure 43. Again, this drop is acceptable. The polarizations are as expected with a 10 dB difference in L-band between cross and linear.

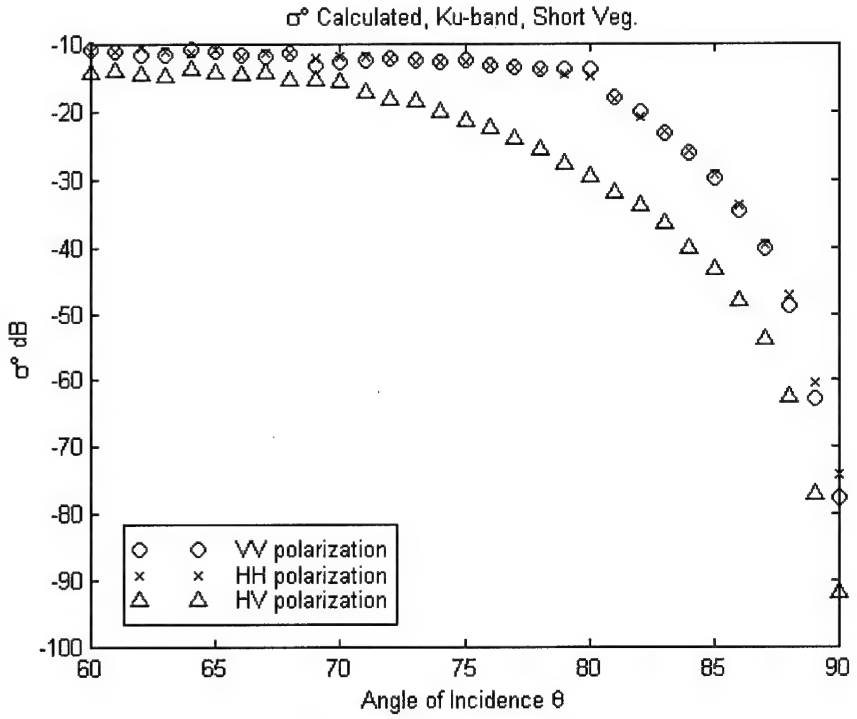

Figure 42. Ku-Band

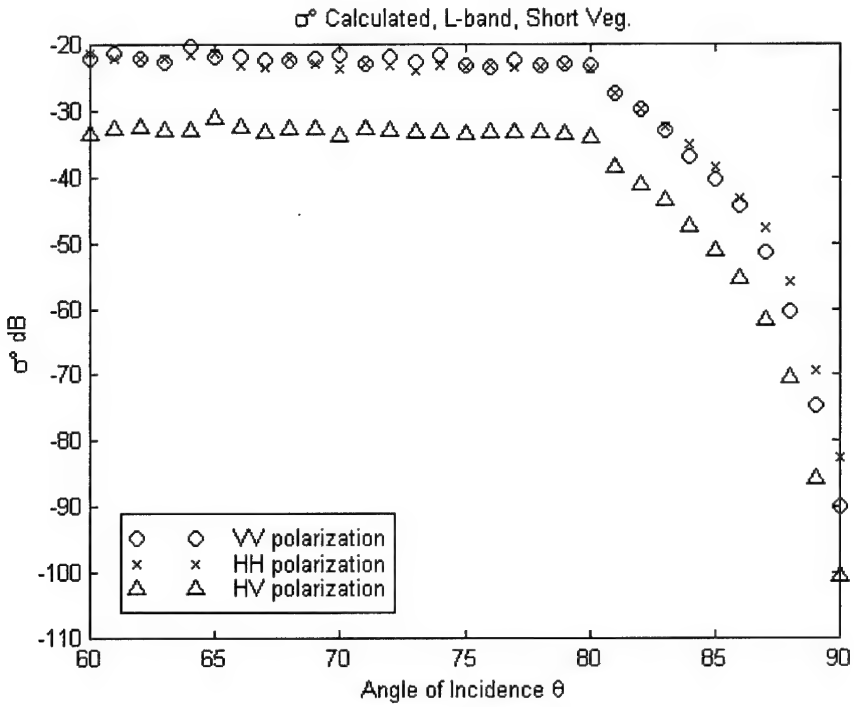

Figure 43. L-Band

4.2.6 Roads (RADLAB Surface F).

Roads sea state is set very low at 0.5 since the surface is usually smooth. The curvature shape matches well to the measured data. The HH polarization is lower than expected, (closer to HV than to VV) however it is still acceptable.

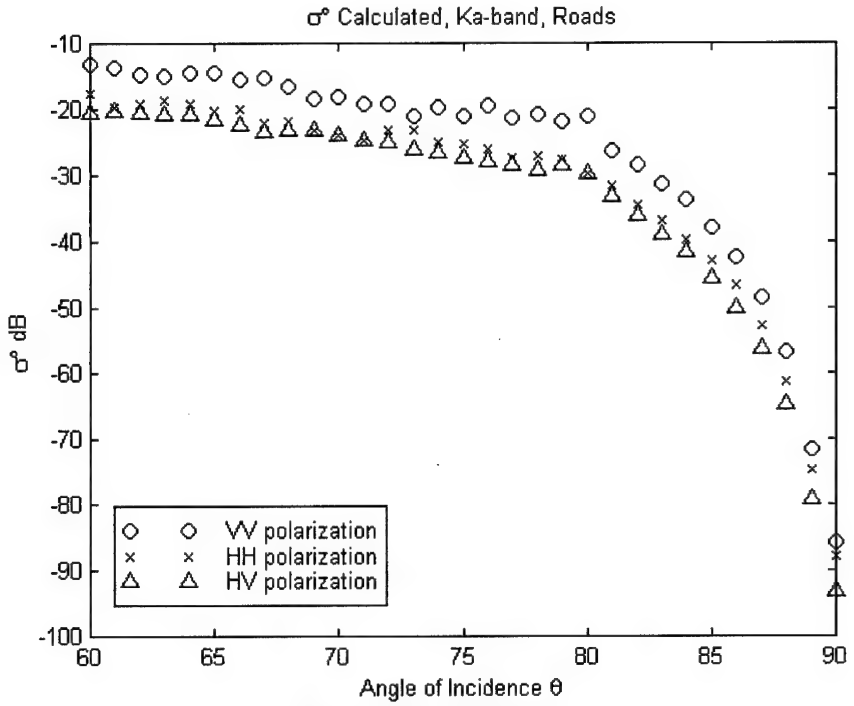

Figure 44. Ka-Band

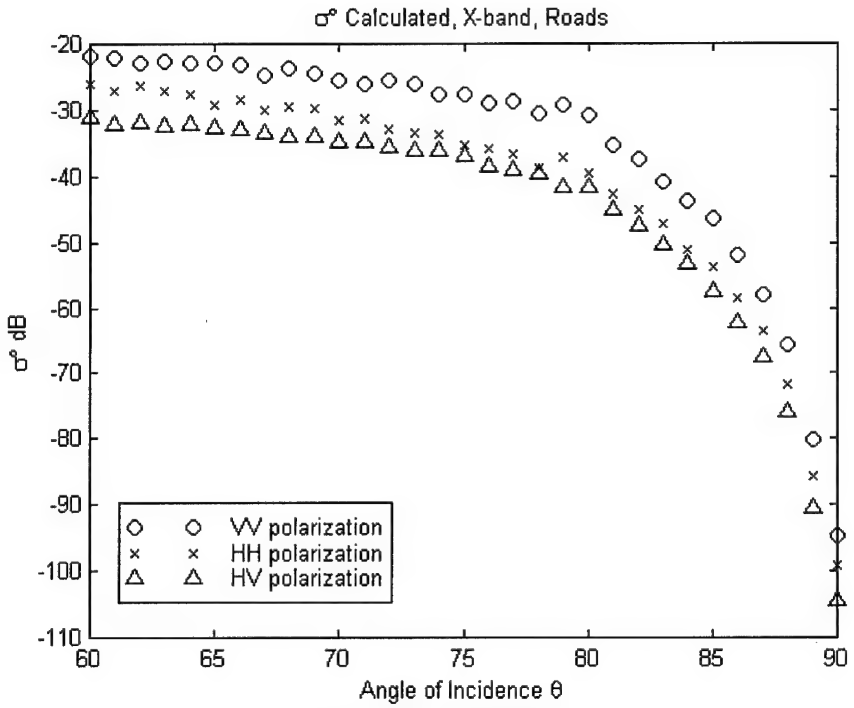

Figure 45. X-Band

4.2.7 Urban Areas (RADLAB Surface G).

Urban areas are only included for experimental purposes. Mediavilla feels the measurements sample size is too small and too erratic to be accurate [2]. He recommends a larger data set needs to be measured before the model is accuate. The sea state is set at 6.0 but can be changed with new validation data.

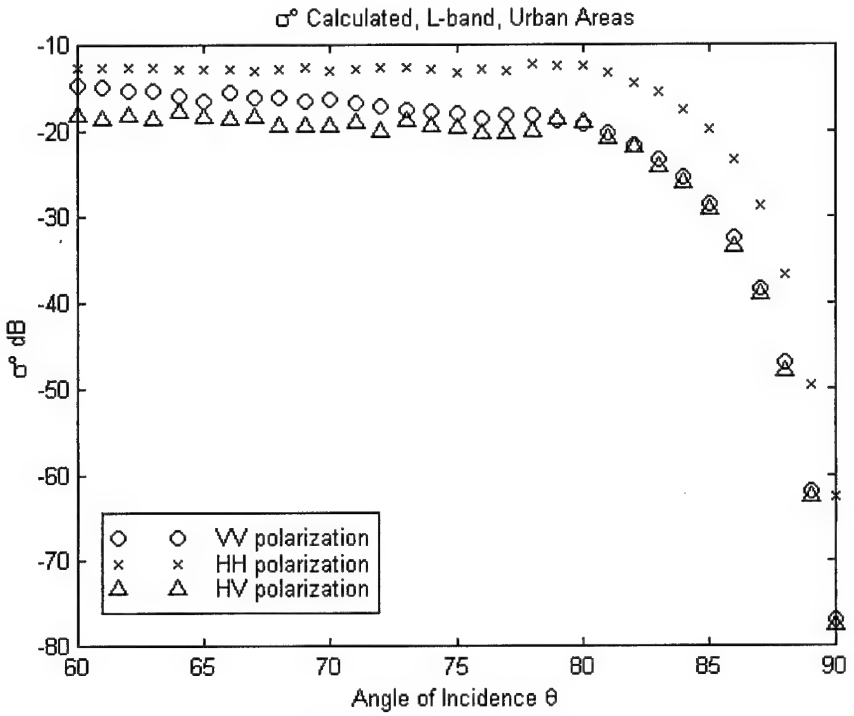

Figure 46. L-Band

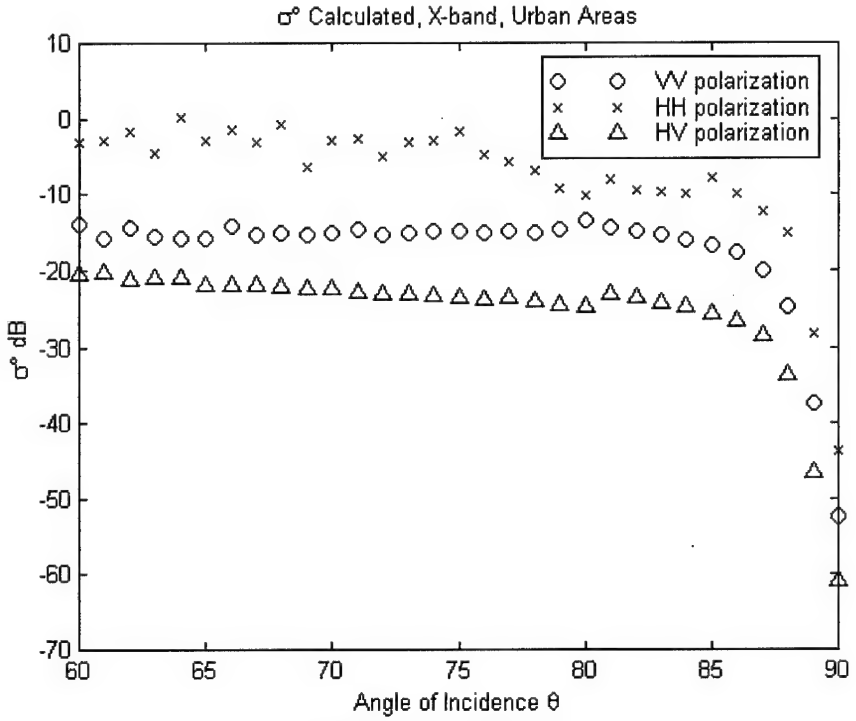

Figure 47. X-Band

4.2.8 Dry Snow (RADLAB Surface H).

For both dry and wet snow, the curvature and polarizations perform as expected. The sea state for dry snow is set to 0.5 due to its general surface smoothness.

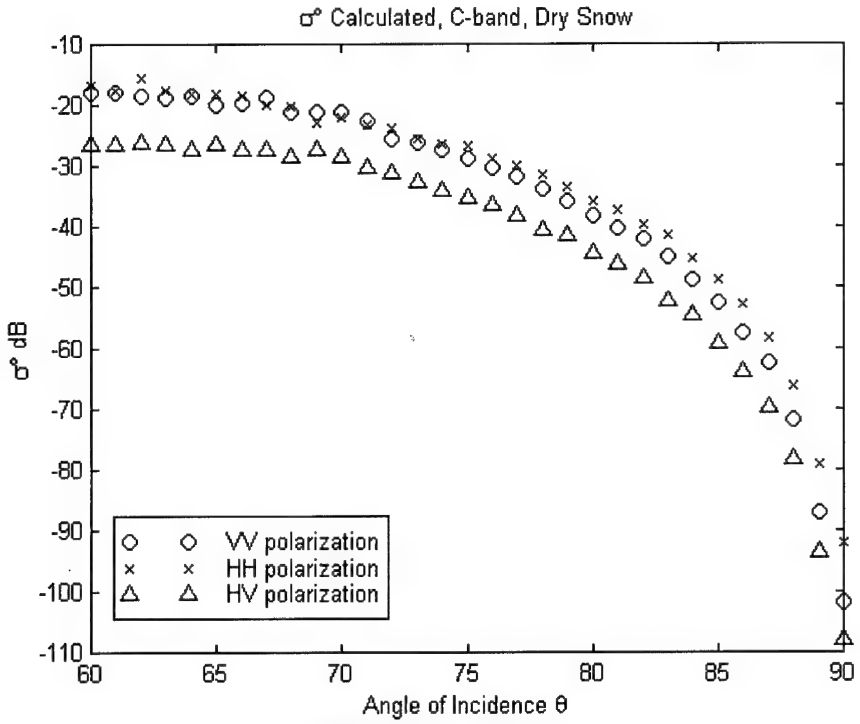

Figure 48. C-Band

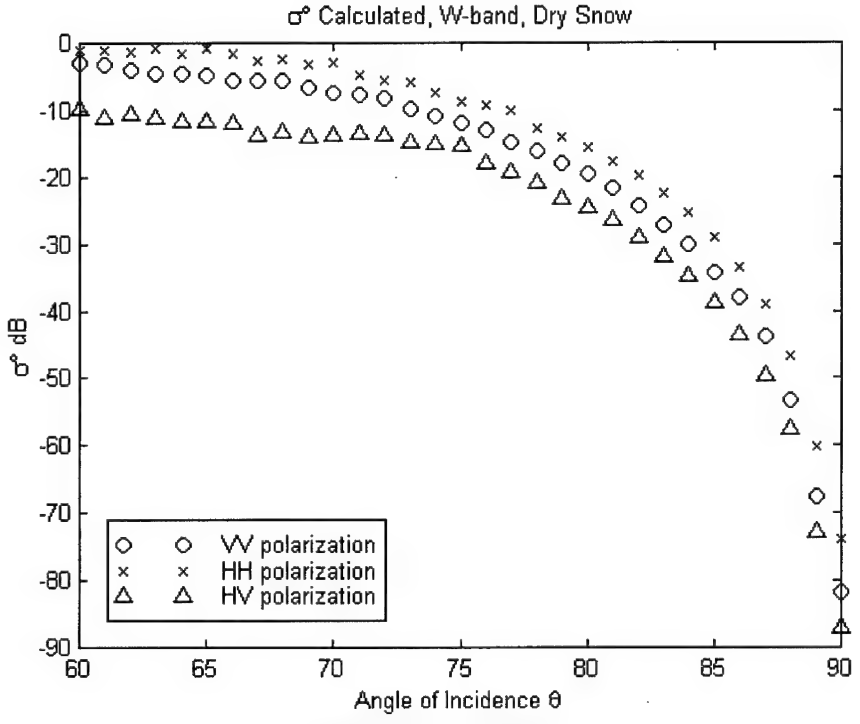

Figure 49. W-Band

4.2.9 Wet Snow (RADLAB Surface I).

As stated before, the curvature and polarizations are as expected. The sea state for wet snow is 0.6, slightly higher than dry snow. This is due to the higher mositure content of wet snow which has been shown to result in a higher σ^o when compared to dry snow [1, 7].

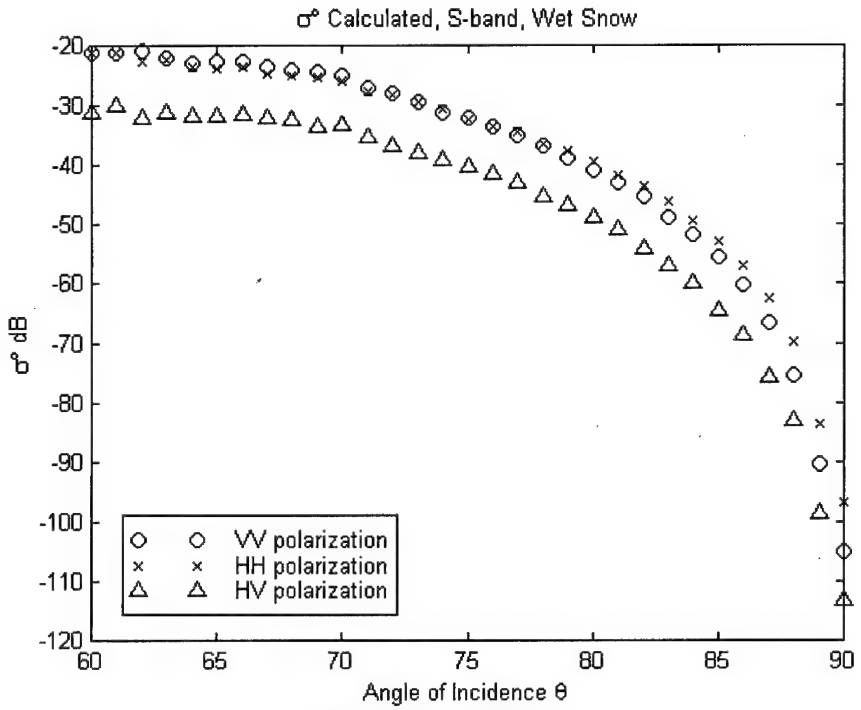

Figure 50. S-Band

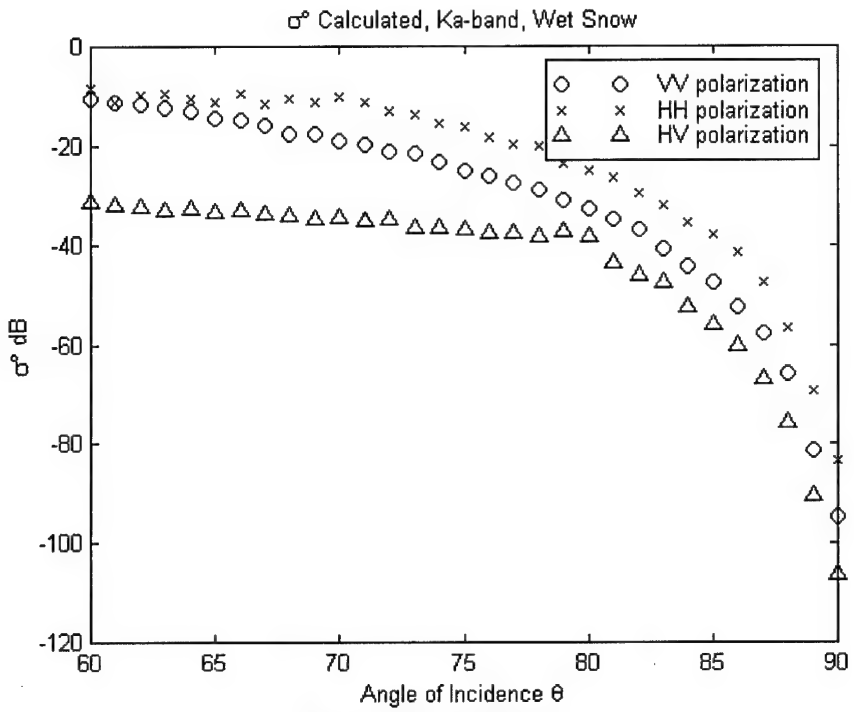

Figure 51. Ka-Band

V. Conclusions and Recommendations

A complete incidence angle σ^o model, σ_{WMOC} **GEN**, for use in terrain modeling simulations was developed and tested.

Having measured data for only four surface types at one frequency makes it very difficult to validate the final model. Still, this is the **first** σ^o model for incidence angles $0^o \leq \theta \leq 90^o$ for multiple terrain types and frequency bands. Any new, measured data will serve only to improve this model.

Military applications for this final model are numerous. This model was originally developed for backscatter removal from simulated radar returns for improved target detection. This model is not limited to backscatter removal but can also be used if the backscatter is the target. When matched with DTED data, terrain identification can assist with ground operations. Finally, surveillance on crops and forest conditions can be quickly completed, giving potential dry conditions where wildfires could become a threat. Other uses will be identified as the model improves.

The final model works as specified. However, there are several ways to improve it. Recommendations for future works include:

1. Perform a complete remeasurement of the nine terrain types in the full angular range (0^o – 90^o) in the 7 radar bands using at least two different radars in the same test. The use of two different radars will allow for the removal of any constants introduced due to registration errors.

2. Introduce a propagation model to the low-grazing portion of the model. A system from John Hopkins is used by the Navy to provide site-specific σ^o measurements based on DTED data and a propagation model. The system works by sending a series of pulses at an area and processing the returns through a propagation model to remove any atmospheric effects. Then, using DTED data for the area observed, the system measures the σ^o returned from that terrain. The measured σ^o is then used to remove backscatter energy from subsequent pulse returns. This system suffers from problems with inaccurate weather forecasts, inaccurate DTED data, and the possibility of extra targets not on the DTED data being measured and excluded [11]. A compilation of this final model and the John Hopkins system could result in a more complete model.
3. Research the vector cross-polarization terms. This research assumed that the cross-polarization terms, σ^o_{VH} and σ^o_{HV}, were simple polarizations. However, there are vector cross-polarization terms which affect how the transmitted and received energies relate [4, 13].

Appendix A. Terrain Backscatter Code in MATLAB®

A.1 Introduction

The following two functions are included as a reference for the figures and equations described in this work. The WMOC function (Wilson, Mediavilla, and O'Connor) is the main function that calls Wilson/Mediavilla Weibull function and the Seamodel function. The reader is recommended to read Mediavilla [2] on the creation and format of the Weibull coefficient table that is the basis of the function.

MATLAB® was chosen as the programming language due to its ease and availability. A FORTRAN® program, based on these functions, is available from the author and AFRL/SNAS.

A.2 WMOC Function

```
function sigmadb = wmoc(angle,frequency,terrain,polarization)
% WMOC Wilson, Mediavilla, O'Connor Terrain Backscatter Generator
% Written 23 Mar 99
% WMOC will return a backscatter sigma value for a given incidence
%       angle (degrees), frequency (IEEE/ANSI STD 527), terrain type
%       (RADLAB nomenclature), and polarization (HH, VV, HV)
% S = WMOC(angle, frequency, terrain, polarization)

% Load terrain file to determine highest measurement incidence angle
% Nomenclature e (terrain type) w (frequency band) vv (polarization)
% See Mediavilla for terrain file creation and format.
load ewvv

% Determine maximum measured incidence angle
maxangle =  max(uldo(:,6));


if angle <= maxangle
  %If the requested angle has measured data
```

```
  %Generate a random number
  U = rand(1);

  %Retrieve alpha, beta, and gamma of Weibull distribution for
  %the requested angle
  row = find(uldo(:,6)==angle);
    alpha = uldo(row,12);
    beta = uldo(row,13);
  gama = uldo(row,14);

  %Calculate Sigma
  sigma = beta*((-log(U)).^alpha)+gama;

  %Convert to dB and return
    sigmadb = 20*log10(sigma);

else
  %If the requested angle does not have measured data

  switch upper(frequency)
    case 'L',  freq = 1.5e9;
    case 'S',  freq = 3.0e9;
    case 'C',  freq = 6.0e9;
    case 'X',  freq = 10.0e9;
    case 'KU', freq = 15e9;
    case 'KA', freq = 35e9;
    case 'W',  freq = 95e9;
    otherwise, disp('Unknown Frequency Band.')
    end

  switch upper(terrain)
    case 'A', sea = 0.8; % Soils & Rock Surfaces
    case 'B', sea = 3.0; % Trees
    case 'C', sea = 1.0; % Grass
    case 'D', sea = 1.7; % Shrubs
    case 'E', sea = 1.3; % Short Vegetation
    case 'F', sea = 0.5; % Roads
    case 'G', sea = 6.0; % Urban Area
    case 'H', sea = 0.5; % Dry Snow
    case 'I', sea = 0.6; % Wet Snow
    otherwise, disp('Unknown Terrain Type.')
    end

   switch upper(polarization)
```

```
  case 'VV', pole = 0; % Vertical-Vertical
  case 'HH', pole = 1; % Horizontal-Horizontal
  case 'HV', pole = 0; % Horizontal-Vertical
  case 'VH', pole = 1; % Vertical-Horizontal
  otherwise, disp('Unknown Polarization Type.')
  end

% Sea model does not work at horizon.  Value at horizon
% is set at 0.1 degrees below horizon
if angle == 90
  sigmadb = seamodel(89.9,sea,freq,pole);
else
  sigmadb = seamodel(angle,sea,freq,pole);
end

% Set measured data plateau for sea model to start from

 % Calculate first point of measured data vs sea model
  % Generate a random number
  U = rand(1);

  % Retrieve alpha, beta, and gamma of Weibull distribution for
  % the requested angle
  row = find(uldo(:,6)==maxangle);
    alpha = uldo(row,12);
    beta = uldo(row,13);
  gama = uldo(row,14);

  % Calculate Sigma
  sigma = beta*((-log(U)).^alpha)+gama;

  plateau(1) = 20*log10(sigma) - seamodel(maxangle,sea,freq,pole);

% Calculate second point of measured data vs sea model
 % Generate a random number
 U = rand(1);

 % Retrieve alpha, beta, and gamma of Weibull distribution for
 % the requested angle
 row = find(uldo(:,6)==(maxangle-1));
 alpha = uldo(row,12);
 beta = uldo(row,13);
 gama = uldo(row,14);

 % Calculate Sigma
```

```
    sigma = beta*((-log(U)).^alpha)+gama;

    plateau(2) = 20*log10(sigma) - seamodel(maxangle-1,sea,freq,pole);

  % Calculate third point of measured data vs sea model

    % Generate a random number
    U = rand(1);

    % Retrieve alpha, beta, and gamma of Weibull distribution for
    % the requested angle
    row = find(uldo(:,6)==(maxangle-1));
      alpha = uldo(row,12);
      beta = uldo(row,13);
    gama = uldo(row,14);

    % Calculate Sigma
    sigma = beta*((-log(U)).^alpha)+gama;

      plateau(3) = 20*log10(sigma) - seamodel(maxangle-2,sea,freq,pole);

  % Average three points and combine sigmadb
  sigmadb = sigmadb + mean(plateau);

end

return
```

A.3 SEAMODEL Function

```
function sigmadb = seamodel(angle,wndsp,freq,pole)
% GIT water model as written in ALARM 91 NPS
% Written 23 Mar 99
% Capt Bill O'Connor Thesis work for AFRL/MBV Lab (Capt Kelce Wilson)
% Seamodel will return a sea clutter coefficient based on model
% developed by Horst at el. (Georgia Tech ,1978) for a given incidence
% angle (degrees), wind speed (m/s), frequency (Hz), and polarization
% (vertical or horizontal)
% S = SEAMODEL(angle,wind speed, frequency, polarization)
% Developed in conjunction with WMOC model (WMOC.M)

% Sea Model works on grazing angle nomenclature (horizon = 0)
angle = 90-angle;
```

```
% Convert to radians
angle = angle .* (pi./180);

% Set direction of wind to across the beam.  Curves work best
% in this configuration
wnddir = (pi./2);

% Calculate light wavelength & average water wave height in m
lambda = 299792500/freq;
wave_height = 0.348.*(wndsp./11).^1.8;

if lamda >= 0.03  % freq <= 10 GHz

  % Multipath Interference
  rough = (14.4 .* lamda + 5.5) .* (angle .* wave_height)./lambda;
  A_i = (rough.^4)./(1 + (rough.^4));

  % Interference due to Wind Speed (or wave height)
  Q = 1.1.*(lambda+ 0.2).^(-0.4);
  A_w = ((1.94 .* wndsp)./(1 + wndsp./15)).^Q;

  % Interference due to wind direction ( or wave direction)
  A_u = exp(0.2.*cos(wnddir).*(1 - 2.8 .* angle).*((lambda+0.02).^(-0.4)));

  % Calculate sigma
  sigmah=10.*log10(3.9e-6.*lambda.*(angle.^0.4).*A_i.*A_u.*A_w);

  if pole == 1  % Horizontal Polarization
    sigmadb = sigmah;
  else        % Vertical Polarization
    if lamda <= 0.01 % freq > 3 GHz
      sigmadb = sigmah - 1.05.*log(wave_height+0.02)+1.09.*log(lambda)...
        +1.27.*log(angle+0.001)+9.7;
    else
      sigmadb = sigmah - 1.73.*log(wave_height+0.02)+3.76.*log(lambda)...
        +2.46.*log(angle+0.001)+22.2;
    end

  end

else %Freq > 10GHz

  Q = 1.93.*(lambda+ 0.2).^(-0.4);
  A_w = ((1.94 .* wndsp)./(1 + wndsp./15)).^Q;
```

```
  rough = (14.4 .* lambda +5.5) .* (angle .* wave_height)./lambda;

  A_i = (rough.^4)./(1 + (rough.^4));

  A_u = exp(0.25.*cos(wnddir).*(1 - 2.8 .* angle).*((lambda).^(-0.33)));

  sigmah = 10.*log10(5.8e-6.*(angle.^0.47).*A_i.*A_u.*A_w);

  if pole == 1  % Horizontal Polarization
    sigmadb = sigmah;
  else        % Vertical Polarization
    sigmadb = sigmah - 1.38.*log(wave_height)+3.42.*log(lambda)...
        +1.31.*log(angle)+18.55;
  end


end

return
```

Bibliography

1. Ulaby, Fawwaz T. & Dobson, M. Craig, Handbook of Radar Scattering Statistics for Terrain, Artech House, 1989.

2. Mediavilla, Ricardo, Terrain Backscatter Generator, Masters Thesis, AFIT/GE/ENG/99M-18, Air Force Institute of Technology (AU), Wright-Patterson AFB, OH, March 1999.

3. Currie, Nicholas et al., Millimeter-Wave Radar Clutter, Artech House, 1992.

4. Long, Maurice W., Radar Reflectivity of Land and Sea, Lexington Books, 1975.

5. Mosher, Terry D., Improvements to the Advanced Low Altitude Radar Model (ALARM 91), Masters Thesis, Naval Postgraduate School, Monterey, CA, September 1992.

6. R. Wellman et al., Analyses of millimeter wave radar low-angle ground-clutter measurements for European-like and desert environments, Army Research Laboratory, Adelphi, MD, Tech Rep ARL-TR-1102, Jan 1996.

7. Ulaby et al. "95-GHz Scattering by Terrain at Near-Grazing Incidence", IEEE Transactions on Antenna and Propagation, Jan 1998.

8. Eaves, Jerry L. & Reedy, Edward K., Principles of Modern Radar, Van Nostrand Reinhold Company, 1987.

9. Skolnik, Merril I., Radar Handbook, McGraw Hill, 1990.

10. Wilson, Kelce S., Effects of Clutter Height Distribution on Adaptive Clutter Erasure Performance, Ph.D. dissertation, AFIT/DS/ENG/98-05, Air Force Institute of Technology (AU), Wright-Patterson AFB, OH, June 1998.

11. Lin, Christopher C. & J. Patrick Reilly, "A Site-Specific Model of Radar Terrain Backscatter and Shadowing", John Hopkins APL Technical Digest, Volume 18, Number 3, 1997.

12. Long, Pg 33

13. Wilson, Kelce, Verbal and written communications, May 1998- February 1999.

14. Beckmann, Petr and Andre Spizzichino, The Scattering of Electromagnetic Waves from Rough Surfaces, Artech House, 1987.

15. Horst, M.M. et al., "Radar Sea Clutter Model", International Conference on Antennas and Propagation, Part 2, 1978.

Vita

William O'Connor was born on 26 July 1972 in Milwaukee, WI. Upon receiving his diploma from Sheboygan North High School, he attended Marquette University, Milwaukee, WI on an Air Force ROTC scholarship. William graduated with a Bachelor of Science degree in Electrical Engineering on 22 May 1994 and was given a Reserve Commission. His first Air Force assignment was at Hanscom AFB, MA for the Computer Acquisition Division, Electronic System Center (ESC/AVC). After a year and half, William was transferred to the Theater Battle Management Core Systems (TBMCS) installation office (ESC/AVB) and was lead installer of TBMCS systems at Whiteman AFB, MO and Dyess AFB, TX. In August 1997, he reported to the Air Force Institute of Technology to begin work on a Master's degree in Electrical Engineering. After graduation, William will be assigned to the 338th Technical Training Squadron, Keesler AFB, MS to be Course Director, Systems Evaluation School.

Permanent Address: 2786 Northwynde Passage
Sun Prairie, WI 53590